

# On the Dynamics of Charged Electromagnetic Particulate Jets

T.I. Zohdi

Received: 22 August 2009 / Accepted: 22 August 2009 / Published online: 30 March 2010  
© CIMNE, Barcelona, Spain 2010

**Abstract** This work addresses the modeling and simulation of charged particulate jets in the presence of electromagnetic fields. The presentation is broken into two main parts: (1) the dynamics of charged streams of particles and their interaction with electromagnetic fields and (2) the coupled thermal fields that arise within the jet. An overall model is built by assembling submodels of the various coupled physical events to form a system that is solved iteratively. Specifically, an approach is developed whereby the dynamics of charged particles, accounting for their collisions, inter-particle near-fields, interaction with external electromagnetic fields and coupled thermal effects are all computed implicitly in an iterative, modular, manner. A staggered, temporally-adaptive scheme is developed to resolve the multiple fields involved and the drastic changes in the physical configuration of the stream, for example when impacting a solid wall or strong localized electromagnetic field. Qualitative analytical results are provided to describe the effects of the electromagnetic fields and quantitative numerical results are provided for complex cases.

## 1 Introduction

Many modern manufacturing processes, in particular those involved in the fabrication of small-scale devices, employ concentrated microscale particulate flows, in the form of jet-sprays, streams, etc. Processes such as ablation, epi-

taxy, sputtering, etc., are commonplace.<sup>1</sup> External electromagnetic fields can be utilized to manipulate and control such particulate flows in order to achieve results that are not possible by purely mechanical means alone. Industrial applications where this is important include electrostatic copiers, inkjet printers, powder coating machines, aerosol design, etc. Furthermore, several industrial processes, such as Chemical Mechanical Planarization (CMP), involve using small-scale chemically-reacting particulates to ablate rough small-scale surfaces flat. These technologies have become important for the success of many micro- and nanotechnologies (Luo and Dornfeld [85–88]). *It is estimated that over 50% (by weight) of the materials used in high-end technology start out as particles or granulated material.* However, at small scales, particulates exhibit strong sensitivity to near-field forces, which are an outcome of electromagnetic forces between ions, leading to agglomeration (“clustering”) and manufacturing inconsistencies that can strongly affect the overall product quality (Fig. 1).<sup>2</sup> Below a certain particle length-scale, approximately one millimeter, the dynamics of particles can be strongly affected inter-particle near-field forces and external electromagnetic fields. In some cases, the near-field forces could be due to “stray” (unwanted) electromagnetic effects or a result of induced/controlled electromagnetic fields. During processing, whether intended or not, particulate agglomeration can occur. The formation of those clusters in the presence of an electromagnetic field are also of high interest because they may lead to poor spray quality and inconsistent fabrication

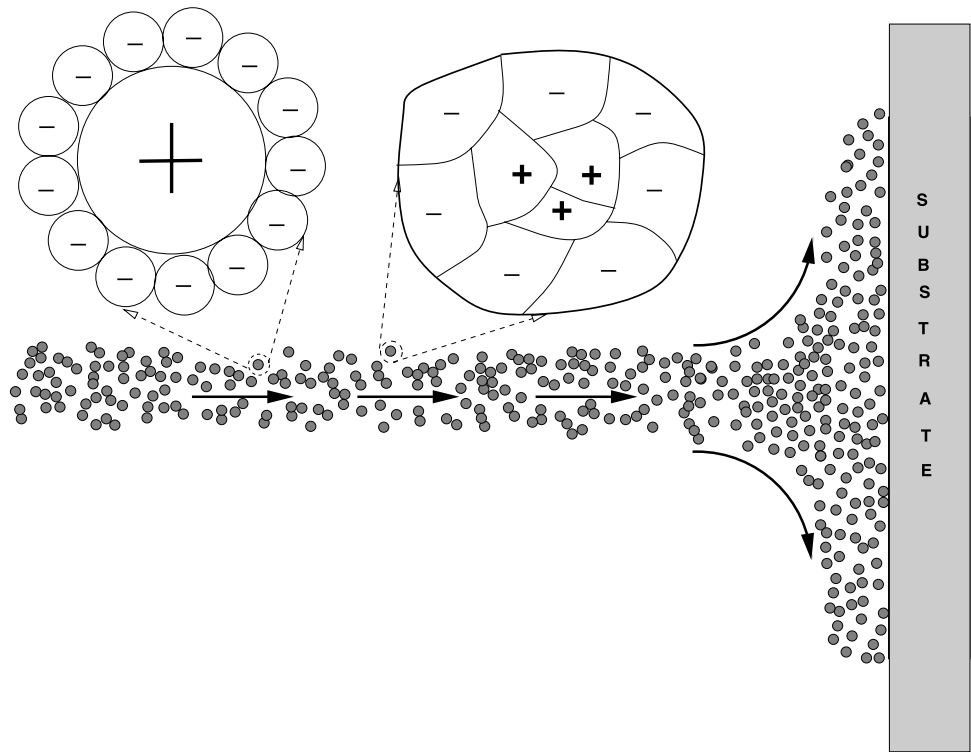
---

T.I. Zohdi (✉)  
Department of Mechanical Engineering, University of California,  
6195 Etcheverry Hall, Berkeley, CA, 94720-1740, USA  
e-mail: [zohdi@me.berkeley.edu](mailto:zohdi@me.berkeley.edu)

<sup>1</sup>The term “particulate” implies small-scale particles. We shall use the terms “particle” and “particulate” interchangeably throughout this work.

<sup>2</sup>The combination of attraction and repulsion forces is denoted as a “near-field” force.

**Fig. 1** Processing of a surface with a particulate spray. Applications can vary from (1) epitaxy (particle lay-up), (2) particle embedding/infiltration and (3) ablation. Complex (charged particle-charged particle (ion-ion)) interaction results in effective interaction that have attractive and repulsive components



results. Therefore, neglecting such near-field effects in an analysis can lead to a significant miscalculation of the characteristics of such flows. The modeling and simulation of the dynamics of small-scale particulate flows in the presence of near-fields and electromagnetic fields, which leads to cluster formation, are the main part of this work.

*Remarks* The study of uncharged “granular” or “particulate” media, in the absence of electromagnetic effects, is wide ranging. Classical examples include the study of natural materials, such as sand and gravel, associated with coastal erosion, landslides and avalanches. For reviews, see Pöschel and Schwager [113], Duran [27], Jaeger and Nagel [53, 54], Nagel [99], Liu et al. [83], Liu and Nagel [84], Jaeger and Nagel [55], Jaeger et al. [56–58], Jaeger and Nagel [59], the extensive works of Hutter and collaborators: Tai et al. [128–130], Gray et al. [37], Wieland et al. [136], Berezin et al. [15], Gray and Hutter [38], Gray [39], Hutter [46], Hutter et al. [47], Hutter and Rajagopal [48], Koch et al. [72], Greve and Hutter [40] and Hutter et al. [49]; the works of Behringer and collaborators: Behringer [12], Behringer and Baxter [11], Behringer and Miller [13] and Behringer et al. [14]; the works of Jenkins and collaborators: Jenkins and Strack [60], Jenkins and La Ragione [61] Jenkins and Koenders [62], Jenkins et al. [63] and the works of Torquato and collab-

orators: Torquato [132], Kansa et al. [67] and Donev et al. [22–26].<sup>3</sup>

## 2 PART I: Jets with Inter-particle Near-fields

### 2.1 Near-field Interaction

In order to motivate the near-field interaction that is often present between particulates (small-scale particles), we recall that the force between two electrically charged particles is given by (Coulomb’s law)

$$\Psi^e = \frac{q_i q_j}{4\pi\epsilon \|\mathbf{r}_i - \mathbf{r}_j\|^2} \mathbf{n}_{ij} \quad (2.1)$$

where  $\Psi^e$  is the force acting between the particles,  $q_i$  is the charge of particle  $i$ ,  $q_j$  is the charge of particle  $j$ ,  $\epsilon$  is the permittivity and  $\mathbf{n}_{ij}$  is the normal direction, determined by the difference in the position vectors of the particles’ centers, defined by

$$\mathbf{n}_{ij} \stackrel{\text{def}}{=} \frac{\mathbf{r}_j - \mathbf{r}_i}{\|\mathbf{r}_i - \mathbf{r}_j\|}, \quad (2.2)$$

<sup>3</sup>In the manufacturing of particulate composite materials, small-scale particles, which are transported and introduced into a molten matrix play a central role. For example, see Aboudi [1], Hashin [43], Mura [98], Nemat-Nasser and Hori [100], Torquato [132] and Zohdi and Wrighers [157].

where  $\|\mathbf{r}_i - \mathbf{r}_j\|$  is the separation distance between particles  $i$  (located at  $\mathbf{r}_i$ ) and  $j$  (located at  $\mathbf{r}_j$ ) and  $\|\cdot\|$  represents the Euclidean norm in  $R^3$ . Usually, one writes  $\epsilon = \epsilon_o \epsilon_r$  where  $\epsilon_o = 8.854 \times 10^{-12}$  farads/meter is the free space permittivity and  $\epsilon_r$  is the relative permittivity or “dielectric” constant. For point charges of like sign, the Coulombic force is one of repulsion, while for opposite charges the force is attractive. We also recall the important observations in conjunction with electromagnetic phenomena (Jackson [52]):

- If a point charge  $q$  experiences a force  $\Psi^e$ , the electric field,  $\mathbf{E}$ , at a position of the charge is defined by  $\Psi^e = q\mathbf{E}$ .
- If the charge is moving, another force may arise,  $\Psi^m$ , which is proportional to its velocity  $\mathbf{v}$ . This other field is denoted as the “magnetic induction” (induced) or just the “magnetic field”,  $\mathbf{B}$ , such that  $\Psi^m = q\mathbf{v} \times \mathbf{B}$ .
- If the forces occur concurrently (the charge is moving through the region possessing both electric and magnetic fields), then  $\Psi = q\mathbf{E} + q\mathbf{v} \times \mathbf{B}$ .

While, in theory, Maxwell’s equations can be applied at the scale of each component within a collection of (charged) particulate ions (Fig. 1), the system of equations would become so massive that its solution would be out of reach of virtually all computers available within the near future. For this reason, empirically-generated interaction laws for complex particulate ion-ion interaction, resulting in effective interaction that have attractive and repulsive components, are employed (Fig. 1). The electric field induced on a particle  $i$  by a particle  $j$ , is a result of interaction between complex aggregates of positive and negative charges together. A simple form that captures the essential features is

$$\Psi_i^{nf} = \sum_{j \neq i}^{N_p} \left( \underbrace{\alpha_{1ij} \|\mathbf{r}_i - \mathbf{r}_j\|^{-\beta_1}}_{\text{attraction}} - \underbrace{\alpha_{2ij} \|\mathbf{r}_i - \mathbf{r}_j\|^{-\beta_2}}_{\text{repulsion}} \right) \underbrace{\mathbf{n}_{ij}}_{\text{unit vector}}, \quad (2.3)$$

where the  $\alpha$ ’s and  $\beta$ ’s are empirical material parameters.

*Remark 2.1* The various representations (decompositions) of the coefficients that appear in (2.3) are, with  $c_i = \pm 1$  (a positive/negative identifier),

- mass-based ( $m = \text{mass}$ ):  $\alpha_{ij} = \bar{\alpha}_{ij} m_i m_j c_i c_j$ ,
- surface area-based ( $a = \text{surface area}$ ):  $\alpha_{ij} = \bar{\alpha}_{ij} a_i a_j c_i c_j$ ,
- volume-based ( $V = \text{volume}$ ):  $\alpha_{ij} = \bar{\alpha}_{ij} V_i V_j c_i c_j$  and
- charge-based:  $\alpha_{ij} = \bar{\alpha}_{ij} q_i q_j c_i c_j$ ,

where the  $\bar{\alpha}_{ij}$  are empirical material parameters. When a particle is relatively large, over essentially a millimeter,

near-fields are quite small, in comparison with other forces. However, below one millimeter, a combination of the various near-field effects, positive and negative charge distributions, etc., can lead to a composite, or “effective” near-field, composed of an attractive and repulsive force (2.3).

*Remark 2.2* We will utilize the decomposition of the electromagnetic forces generated into a (inter-particle) near-field interaction and the external electromagnetic field

$$\Psi_i = \underbrace{\sum_{j \neq i}^N \Psi_{ij}^{nf}}_{\Psi_i^{nf}} + \Psi_i^{ext} = \Psi_i^{nf} + \underbrace{q_i(\mathbf{E}^{ext} + \mathbf{v}_i \times \mathbf{B}^{ext})}_{\Psi_i^{env}}, \quad (2.4)$$

where  $\sum_{j \neq i}^N \Psi_{ij}^{nf}$  represents the interaction between particle  $i$  and all other particles  $j = 1, 2, \dots, N$  ( $j \neq i$ ),  $\mathbf{E}^{ext}$  and  $\mathbf{B}^{ext}$  are externally-controlled fields that are independent of the response of the system.  $\mathbf{E}^{ext}$  and  $\mathbf{B}^{ext}$  can be considered as static (or extremely slowly-varying), and thus uncoupled and independently controllable. The self-induced induced magnetic fields developed between particles is insignificant for the velocity ranges of interest here (well below the speed of light). Other forces, such as contact and friction will be introduced shortly.

*Remark 2.3* The specific structure of the near-field interaction law chosen was only one of many possibilities to model near-field behavior. There are vast numbers of empirical representations, for example, found in the field of “Molecular Dynamics” (MD), which typically refers to mathematical models of systems of atoms or molecules where each atom (or molecule) is represented by a material point in  $R^3$  and is treated as a point mass. The overall motion of such mass-point systems is dictated by Newtonian mechanics. For an extensive survey of MD-type interaction forces, which includes comparisons of the theoretical and computational properties of a variety of interaction laws, we refer the reader to Frenklach and Carmer [33]. In the usual MD approach (see Haile [41], for example), the motion of individual atoms is described by the Newton’s second law with the forces computed from differentiating a prescribed potential energy function, with applications to solids, liquids, and gases, as well as biological systems (Hase [42], Schlick [120] and Rapaport [117]). The interaction functions usually take the form of the familiar Mie, Lennard-Jones, and Morse potentials (Moelwyn-Hughes [94]), however three-body terms can be introduced directly into the interaction functions (Stillinger [125]) or, alternatively, “local” modifications can be made to two-body representations (Tersoff [131]).

### 3 Multiple Particulate Flow in the Presence of Near-fields

The objects in the flow are assumed to be small enough to be considered (idealized) as particles, spherical in shape, and that the effects of their rotation with respect to their mass center is unimportant to their overall motion.

#### 3.1 Particulate Dynamics with Near-fields

We consider a group of non-overlapping particles ( $N_p$  in total). The approach in this section draws from methods developed in Zohdi [148, 150] and [154]. The equation of motion for the  $i$ th particle in a flow is

$$m_i \ddot{\mathbf{r}}_i = \Psi_i^{tot}(\mathbf{r}_1, \mathbf{r}_2, \dots, \mathbf{r}_{N_p}), \tag{3.1}$$

where  $\mathbf{r}_i$  is the position vector of the  $i$ th particle and where  $\Psi_i^{tot}$  represents all forces acting on particle  $i$ . Specifically,

$$\Psi_i^{tot} = \Psi_i^{nf} + \Psi_i^{con} + \Psi_i^{fric} + \Psi_i^{env} \tag{3.2}$$

represents the sum of forces due to near-field interaction ( $\Psi^{nf}$ , introduced in (2.3)), normal contact impulsive forces ( $\Psi^{con}$ ), frictional impulse forces ( $\Psi^{fric}$ ) and the surrounding environment ( $\Psi^{env}$ ).<sup>4</sup>

*Remarks* In many applications the near-fields can dramatically change when the particles are very close to one another, leading to increased repulsion or attraction. A particularly straightforward way to model this is via a near-field attractive/repulsive augmentation of the form

$$\tilde{\Psi}_i^{nf} = \Psi_i^{nf} + \underbrace{\alpha_a \|\mathbf{r}_i - \mathbf{r}_j\|^{\beta_a} \mathbf{n}_{ij}}_{\Psi^{a,def} = \text{augmentation force}}, \tag{3.3}$$

which is activated if

$$\|\mathbf{r}_i - \mathbf{r}_j\| \leq (b_i + b_j)\delta_a, \tag{3.4}$$

where  $b_i$  and  $b_j$  are the radii of the particles, and where  $0 \leq \delta_a$  is the critical distance needed for the augmentation to become active. When  $\delta_a = 1$  and  $\alpha_a < 0$ , then the model can be interpreted as a (contact) penalty for particle interpenetration. Many such ‘‘augmentation’’ models exist. For example see Durand [27]. For many engineering materials,

<sup>4</sup>Such forces can arise from surrounding (gas) fluid (treated in Zohdi [154]) or, as we later discuss, external electromagnetic fields where  $\Psi_i^{env} = q_i(\mathbf{E}^{ext} + \mathbf{v}_i \times \mathbf{B}^{ext})$ .

some surface adhesion persists, which can lead to bonding phenomena between surfaces, even when no explicit external charging has occurred. For example, see Tabor [127] and Rietema [118] (specifically for agglomeration).

#### 3.2 Mechanical Contact with Near-field Interaction

We now consider cases where mechanical contact occurs between particles, in the presence of near-field interaction. A primary simplifying assumption is made: *the particles remain spherical after impact, i.e. any permanent deformation is considered negligible*. For two colliding particles  $i$  and  $j$ , normal to the line of impact, a balance of linear momentum relating the states before impact (time =  $t$ ) and after impact (time =  $t + \delta t$ ) reads as

$$\begin{aligned} m_i v_{in}(t) + m_j v_{jn}(t) &+ \int_t^{t+\delta t} \mathcal{E}_i \cdot \mathbf{n}_{ij} dt + \int_t^{t+\delta t} \mathcal{E}_j \cdot \mathbf{n}_{ij} dt \\ &= m_i v_{in}(t + \delta t) + m_j v_{jn}(t + \delta t), \end{aligned} \tag{3.5}$$

where the subscript  $n$  denotes the normal component of the velocity (along the line connecting particle centers) and the  $\mathcal{E}$ 's represent all forces induced by near-field interaction with other particles, as well as all other external forces, if any, applied to the pair. If one isolates one of the members of the colliding pair, then

$$\begin{aligned} m_i v_{in}(t) + \int_t^{t+\delta t} I_n dt + \int_t^{t+\delta t} \mathcal{E}_i \cdot \mathbf{n}_{ij} dt \\ = m_i v_{in}(t + \delta t), \end{aligned} \tag{3.6}$$

where  $\int_t^{t+\delta t} I_n dt$  is the total normal impulse due to impact. For a pair of particles undergoing impact, let us consider a decomposition of the collision event (Fig. 2) into a compression ( $\delta t_1$ ) and recovery ( $\delta t_2$ ) phase, i.e.  $\delta t = \delta t_1 + \delta t_2$ . Between the compression and recovery phases, the particles

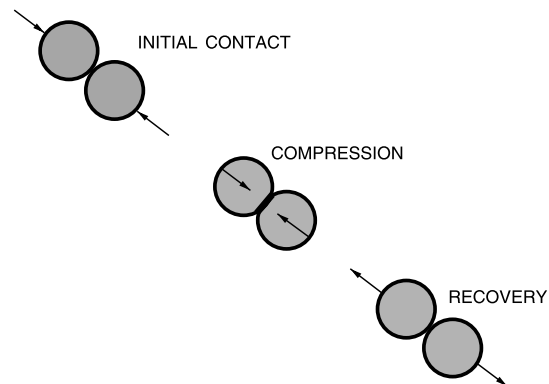


**Fig. 2** Stages of impact: initial contact, compression and recovery of two impacting particles

achieve a common normal velocity,<sup>5</sup> denoted  $v_{cn}$ , at the intermediate time  $t + \delta t_1$ . We may write for particle  $i$ , along the normal, in the compression phase of impact<sup>6</sup>

$$m_i v_{in}(t) + \int_t^{t+\delta t_1} I_n dt + \int_t^{t+\delta t_1} \mathcal{E}_i \cdot \mathbf{n}_{ij} dt = m_i v_{cn}, \tag{3.7}$$

and in the recovery phase

$$m_i v_{cn} + \int_{t+\delta t_1}^{t+\delta t} I_n dt + \int_{t+\delta t_1}^{t+\delta t} \mathcal{E}_i \cdot \mathbf{n}_{ij} dt = m_i v_{in}(t + \delta t). \tag{3.8}$$

For the other particle ( $j$ ), in the compression phase,

$$m_j v_{jn}(t) - \int_t^{t+\delta t_1} I_n dt + \int_t^{t+\delta t_1} \mathcal{E}_j \cdot \mathbf{n}_{ij} dt = m_j v_{cn}, \tag{3.9}$$

and in the recovery phase

$$m_j v_{cn} - \int_{t+\delta t_1}^{t+\delta t} I_n dt + \int_{t+\delta t_1}^{t+\delta t} \mathcal{E}_j \cdot \mathbf{n}_{ij} dt = m_j v_{jn}(t + \delta t). \tag{3.10}$$

This leads to an expression for the coefficient of restitution

$$e \stackrel{\text{def}}{=} \frac{\int_{t+\delta t_1}^{t+\delta t} I_n dt}{\int_t^{t+\delta t_1} I_n dt} = \frac{m_i(v_{in}(t + \delta t) - v_{cn}) - \mathcal{E}_{in}(t + \delta t_1, t + \delta t)}{m_i(v_{cn} - v_{in}(t)) - \mathcal{E}_{in}(t, t + \delta t_1)} = \frac{-m_j(v_{jn}(t + \delta t) - v_{cn}) + \mathcal{E}_{jn}(t + \delta t_1, t + \delta t)}{-m_j(v_{cn} - v_{jn}(t)) + \mathcal{E}_{jn}(t, t + \delta t_1)}, \tag{3.11}$$

where

$$\begin{aligned} \mathcal{E}_{in}(t + \delta t_1, t + \delta t) &\stackrel{\text{def}}{=} \int_{t+\delta t_1}^{t+\delta t} \mathcal{E}_i \cdot \mathbf{n}_{ij} dt, \\ \mathcal{E}_{jn}(t + \delta t_1, t + \delta t) &\stackrel{\text{def}}{=} \int_{t+\delta t_1}^{t+\delta t} \mathcal{E}_j \cdot \mathbf{n}_{ij} dt, \\ \mathcal{E}_{in}(t, t + \delta t_1) &\stackrel{\text{def}}{=} \int_t^{t+\delta t_1} \mathcal{E}_i \cdot \mathbf{n}_{ij} dt, \\ \mathcal{E}_{jn}(t, t + \delta t_1) &\stackrel{\text{def}}{=} \int_t^{t+\delta t_1} \mathcal{E}_j \cdot \mathbf{n}_{ij} dt. \end{aligned} \tag{3.12}$$

<sup>5</sup>A common normal velocity for particles should be interpreted as indicating that the relative velocity in the normal direction between particle centers is zero.

<sup>6</sup>We assume that the ‘‘instantaneous’’ impact events do not occur at the same instant and that their action can be additively collected together within a time step.

If we eliminate  $v_{cn}$ , we obtain an expression for  $e$

$$e = \frac{v_{jn}(t + \delta t) - v_{in}(t + \delta t) + \Gamma_{ij}(t + \delta t_1, t + \delta t)}{v_{in}(t) - v_{jn}(t) + \Gamma_{ij}(t, t + \delta t_1)}, \tag{3.13}$$

$$\begin{aligned} \Gamma_{ij}(t + \delta t_1, t + \delta t) &\stackrel{\text{def}}{=} \frac{1}{m_i} \mathcal{E}_{in}(t + \delta t_1, t + \delta t) \\ &\quad - \frac{1}{m_j} \mathcal{E}_{jn}(t + \delta t_1, t + \delta t) \end{aligned} \tag{3.14}$$

and

$$\begin{aligned} \Gamma_{ij}(t, t + \delta t_1) &\stackrel{\text{def}}{=} \frac{1}{m_i} \mathcal{E}_{in}(t, t + \delta t_1) \\ &\quad - \frac{1}{m_j} \mathcal{E}_{jn}(t, t + \delta t_1). \end{aligned} \tag{3.15}$$

Thus, we may rewrite (3.13)<sup>7</sup> as

$$v_{jn}(t + \delta t) = v_{in}(t + \delta t) - \Gamma_{ij}(t + \delta t_1, t + \delta t) + e(v_{in}(t) - v_{jn}(t) + \Gamma_{ij}(t, t + \delta t_1)). \tag{3.16}$$

It is convenient to denote the average force acting on the particle from external sources as

$$\bar{\mathcal{E}}_{in} \stackrel{\text{def}}{=} \frac{1}{\delta t} \int_t^{t+\delta t} \mathcal{E}_i \cdot \mathbf{n}_{ij} dt. \tag{3.17}$$

If  $e$  is explicitly known, then one can write, combining (3.13) and (3.5),

$$\begin{aligned} v_{in}(t + \delta t) &= \frac{m_i v_{in}(t) + m_j(v_{jn}(t) - e(v_{in}(t) - v_{jn}(t)))}{m_i + m_j} \\ &\quad + \frac{(\bar{\mathcal{E}}_{in} + \bar{\mathcal{E}}_{jn})\delta t - m_j(e\Gamma_{ij}(t, t + \delta t_1) - \Gamma_{ij}(t + \delta t_1, t + \delta t))}{m_i + m_j}, \end{aligned} \tag{3.18}$$

and, once  $v_{in}(t + \delta t)$  is known, one can subsequently also solve for  $v_{jn}(t + \delta t)$  via (3.16).

<sup>7</sup>This collapses to the classical expression for the ratio of the relative velocities before and after impact, if the near-field forces are negligible:

$$e \stackrel{\text{def}}{=} \frac{v_{jn}(t + \delta t) - v_{in}(t + \delta t)}{v_{in}(t) - v_{jn}(t)}.$$

*Remark 3.1* Later, it will be useful to define the average impulsive normal contact force between the particles acting during the impact event as

$$\begin{aligned} \bar{I}_n &\stackrel{\text{def}}{=} \frac{1}{\delta t} \int_t^{t+\delta t} I_n dt \\ &= \frac{m_i(v_{in}(t + \delta t) - v_{in}(t))}{\delta t} - \bar{\mathcal{E}}_{in}. \end{aligned} \tag{3.19}$$

In particular, as will be done later in the analysis, when we discretize the equations of motion with a discrete (finite difference) time-step of  $\Delta t$ , where  $\delta t \ll \Delta t$ , we shall define the impulsive normal contact contribution to the total force acting on a particle,  $\Psi_i^{tot} = \Psi_i^{nf} + \Psi_i^{con} + \Psi_i^{fric} + \Psi_i^{emv}$  (3.1), to be

$$\Psi_i^{con} = \frac{\bar{I}_n \delta t}{\Delta t} \mathbf{n}_{ij}. \tag{3.20}$$

Furthermore, at the implementation level, we choose  $\delta t = \gamma \Delta t$ , where  $0 < \gamma \ll 1$  and  $\Delta t$  is the time-step discretization size, which will be introduced later in the work. A typical choice is  $0 < \gamma \leq 0.01$ . Typically, the system is insensitive to  $\gamma$  below 0.01. We assume  $\delta t_1 + \delta t_2 = \delta t_1 + e\delta t_1$ , which immediately allows the following definitions

$$\delta t_1 = \frac{\gamma \Delta t}{1 + e} \quad \text{and} \quad \delta t_2 = \frac{e\gamma \Delta t}{1 + e}. \tag{3.21}$$

These results are consistent with the fact that the recovery time vanishes (all compression and no recovery) for  $e \rightarrow 0$  (asymptotically “plastic”) and, as  $e \rightarrow 1$ , the recovery time equals the compression time ( $\delta t_2 = \delta t_1$ , asymptotically “elastic”). If  $e = 1$ , there is no loss in energy, while if  $e = 0$  there is a maximum loss in energy. For a more detailed analysis of impact duration times, see Johnson [64].

*Remark 3.2* It is obvious that for a deeper understanding of the deformation within a particle, it must be treated as a deformable continuum, which will require a spatial discretization, for example using the Finite Element Method of the body (particle). For general references on the Finite Element Method, see the well-known books of Bathe [8], Becker, Carey and Oden [9], Hughes [45], Szabo and Babuska [126] and Zienkiewicz and Taylor [141]. For the state of the art in Finite Element Methods, see the recent book of Wriggers [138]. For work specifically focusing on the continuum mechanics of particles, see Zohdi and Wriggers [157]. For a detailed numerical analysis of multifield contact between bodies see Wriggers [137].

#### 4 “Friction” (Resistance to Sliding)

To incorporate frictional stick-slip phenomena during impact for a general particle pair ( $i$  and  $j$ ),<sup>8</sup> the tangential velocities at the beginning of the impact time interval (time =  $t$ ) are computed by subtracting the relative normal velocity away from the total relative velocity:

$$\begin{aligned} \mathbf{v}_{jt}(t) - \mathbf{v}_{it}(t) &= (\mathbf{v}_j(t) - \mathbf{v}_i(t)) \\ &\quad - ((\mathbf{v}_j(t) - \mathbf{v}_i(t)) \cdot \mathbf{n}_{ij}) \mathbf{n}_{ij}. \end{aligned} \tag{4.1}$$

One then writes the equation for tangential momentum change during impact for the  $i$ th particle

$$m_i v_{it}(t) - \bar{I}_f \delta t + \bar{\mathcal{E}}_{it} \delta t = m_i v_{ct}, \tag{4.2}$$

where the friction contribution is

$$\bar{I}_f = \frac{1}{\delta t} \int_t^{t+\delta t} I_f dt, \tag{4.3}$$

where the total contributions from all other particles in the tangential direction ( $\boldsymbol{\tau}_{ij}$ ) are

$$\bar{\mathcal{E}}_{it} = \frac{1}{\delta t} \int_t^{t+\delta t} \boldsymbol{\mathcal{E}}_i \cdot \boldsymbol{\tau}_{ij} dt \tag{4.4}$$

and where  $v_{ct}$  is the common velocity of particles  $i$  and  $j$  in the tangential direction. They do not move relative to one another. Similarly, for the  $j$ th particle we have

$$m_j v_{jt}(t) + \bar{I}_f \delta t + \bar{\mathcal{E}}_{jt} \delta t = m_j v_{ct}. \tag{4.5}$$

There are two unknowns,  $\bar{I}_f$  and  $v_{ct}$ . The main quantity of interest is  $\bar{I}_f$ , which can be solved for

$$\bar{I}_f = \frac{(\frac{\bar{\mathcal{E}}_{it}}{m_i} - \frac{\bar{\mathcal{E}}_{jt}}{m_j})\delta t + v_{it}(t) - v_{jt}(t)}{(\frac{1}{m_i} + \frac{1}{m_j})\delta t}. \tag{4.6}$$

Thus, consistent with stick-slip models of Coloumb friction, one first assumes no slip occurs. If

$$|\bar{I}_f| > \mu_s |\bar{I}_n|, \tag{4.7}$$

where

$$\mu_s \geq \mu_d \tag{4.8}$$

is the coefficient of *static* friction, then slip must occur and a dynamic sliding friction model is used. If sliding occurs,

<sup>8</sup>It is probably more accurate to refer to this as “resistance to sliding” at such small scales, however, for brevity, we refer to the effect as “friction”.

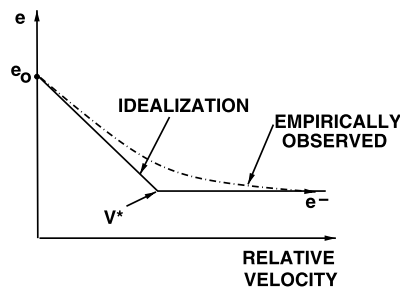


**Fig. 3** Qualitative behavior of the coefficient of restitution with impact velocity (Zohdi [148])

the friction force is assumed to be proportional to the normal force and opposite to the direction of relative tangent motion, i.e.

$$\Psi_i^{fric} \stackrel{\text{def}}{=} \mu_d \|\Psi^{con}\| \frac{\mathbf{v}_{jt} - \mathbf{v}_{it}}{\|\mathbf{v}_{jt} - \mathbf{v}_{it}\|} = -\Psi_j^{fric}. \tag{4.9}$$

### 4.1 Velocity-dependent Coefficients of Restitution

It is important to realize that, in reality, the phenomenological parameter  $e$  depends on the severity of the impact velocity. For extensive experimental data, see Goldsmith [36], or Johnson [64] for a more detailed analytical treatment. Qualitatively, the coefficient of restitution has behavior as shown in Fig. 3. A mathematical idealization of the behavior can be constructed as follows

$$e \stackrel{\text{def}}{=} \max \left( e_0 \left( 1 - \frac{\Delta v_n}{v^*} \right), e^- \right), \tag{4.10}$$

where  $v^*$  is a critical threshold velocity (normalization) parameter and where the relative velocity of approach is defined by

$$\Delta v_n \stackrel{\text{def}}{=} |v_{jn}(t) - v_{in}(t)| \tag{4.11}$$

and  $e^-$  is a lower limit to the coefficient of restitution.

## 5 Iterative Solution Schemes

### 5.1 General Time-stepping Schemes

We now specifically address the second-order systems of interest. The equation of motion is given by

$$m_i \dot{\mathbf{v}}_i = \Psi_i^{tot}, \tag{5.1}$$

where  $\Psi_i^{tot}$  is the total force provided from interactions with the external environment. Expanding the velocity in a Taylor

series about  $t + \phi \Delta t$  we obtain

$$\begin{aligned} \mathbf{v}_i(t + \Delta t) &= \mathbf{v}_i(t + \phi \Delta t) + \left. \frac{d\mathbf{v}_i}{dt} \right|_{t+\phi \Delta t} (1 - \phi) \Delta t \\ &\quad + \left. \frac{1}{2} \frac{d^2\mathbf{v}_i}{dt^2} \right|_{t+\phi \Delta t} (1 - \phi)^2 (\Delta t)^2 + \mathcal{O}(\Delta t)^3 \end{aligned} \tag{5.2}$$

and

$$\begin{aligned} \mathbf{v}_i(t) &= \mathbf{v}_i(t + \phi \Delta t) - \left. \frac{d\mathbf{v}_i}{dt} \right|_{t+\phi \Delta t} \phi \Delta t \\ &\quad + \left. \frac{1}{2} \frac{d^2\mathbf{v}_i}{dt^2} \right|_{t+\phi \Delta t} \phi^2 (\Delta t)^2 + \mathcal{O}(\Delta t)^3. \end{aligned} \tag{5.3}$$

Subtracting the two expressions yields

$$\left. \frac{d\mathbf{v}_i}{dt} \right|_{t+\phi \Delta t} = \frac{\mathbf{v}_i(t + \Delta t) - \mathbf{v}_i(t)}{\Delta t} + \hat{\mathcal{O}}(\Delta t), \tag{5.4}$$

where  $\hat{\mathcal{O}}(\Delta t) = \mathcal{O}(\Delta t)^2$ , when  $\phi = \frac{1}{2}$ . Thus, inserting this into the equations of equilibrium yields

$$\mathbf{v}_i(t + \Delta t) = \mathbf{v}_i(t) + \frac{\Delta t}{m_i} \Psi_i^{tot}(t + \phi \Delta t) + \hat{\mathcal{O}}(\Delta t)^2. \tag{5.5}$$

Note that adding a weighted sum of (5.2) and (5.3) yields

$$\mathbf{v}_i(t + \phi \Delta t) = \phi \mathbf{v}_i(t + \Delta t) + (1 - \phi) \mathbf{v}_i(t) + \mathcal{O}(\Delta t)^2, \tag{5.6}$$

which will be useful shortly. Now expanding the position of the center of mass in a Taylor series about  $t + \phi \Delta t$  we obtain

$$\begin{aligned} \mathbf{r}_i(t + \Delta t) &= \mathbf{r}_i(t + \phi \Delta t) + \left. \frac{d\mathbf{r}_i}{dt} \right|_{t+\phi \Delta t} (1 - \phi) \Delta t \\ &\quad + \left. \frac{1}{2} \frac{d^2\mathbf{r}_i}{dt^2} \right|_{t+\phi \Delta t} (1 - \phi)^2 (\Delta t)^2 + \mathcal{O}(\Delta t)^3 \end{aligned} \tag{5.7}$$

and

$$\begin{aligned} \mathbf{r}_i(t) &= \mathbf{r}_i(t + \phi \Delta t) - \left. \frac{d\mathbf{r}_i}{dt} \right|_{t+\phi \Delta t} \phi \Delta t \\ &\quad + \left. \frac{1}{2} \frac{d^2\mathbf{r}_i}{dt^2} \right|_{t+\phi \Delta t} \phi^2 (\Delta t)^2 + \mathcal{O}(\Delta t)^3. \end{aligned} \tag{5.8}$$

Subtracting the two expressions yields

$$\frac{\mathbf{r}_i(t + \Delta t) - \mathbf{r}_i(t)}{\Delta t} = \mathbf{v}_i(t + \phi \Delta t) + \hat{\mathcal{O}}(\Delta t). \tag{5.9}$$

Inserting (5.6) yields

$$\begin{aligned} \mathbf{r}_i(t + \Delta t) &= \mathbf{r}_i(t) + (\phi \mathbf{v}_i(t + \Delta t) + (1 - \phi) \mathbf{v}_i(t)) \Delta t \\ &\quad + \hat{\mathcal{O}}(\Delta t)^2, \end{aligned} \tag{5.10}$$

and thus using (5.5) yields

$$\begin{aligned} \mathbf{r}_i(t + \Delta t) &= \mathbf{r}_i(t) + \mathbf{v}_i(t)\Delta t + \frac{\phi(\Delta t)^2}{m_i}\Psi_i^{tot}(t + \phi\Delta t) \\ &\quad + \hat{O}(\Delta t)^2. \end{aligned} \tag{5.11}$$

The term  $\Psi_i^{tot}(t + \phi\Delta t)$  can be handled in two main ways:

- $\Psi_i^{tot}(t + \phi\Delta t) \approx \Psi_i^{tot}(\phi\mathbf{r}_i(t + \Delta t) + (1 - \phi)\mathbf{r}_i(t))$  or
- $\Psi_i^{tot}(t + \phi\Delta t) \approx \phi\Psi_i^{tot}(\mathbf{r}_i(t + \Delta t)) + (1 - \phi)\Psi_i^{tot}(\mathbf{r}_i(t))$ .

The differences are quite minute between either of the above, thus, for brevity, we choose the latter, which is a ‘‘trapezoidal’’ rule. In summary, we have the following:

$$\begin{aligned} \mathbf{r}_i(t + \Delta t) &= \mathbf{r}_i(t) + \mathbf{v}_i(t)\Delta t + \frac{\phi(\Delta t)^2}{m_i}(\phi\Psi_i^{tot}(\mathbf{r}_i(t + \Delta t)) \\ &\quad + (1 - \phi)\Psi_i^{tot}(\mathbf{r}_i(t))) + \hat{O}(\Delta t)^2, \end{aligned} \tag{5.12}$$

where

- when  $\phi = 1$ , then this is the (implicit) Backward Euler scheme, which is very stable (very dissipative) and  $\hat{O}(\Delta t)^2 = \mathcal{O}(\Delta t)^2$  locally in time,
- when  $\phi = 0$ , then this is the (explicit) Forward Euler scheme, which is conditionally stable and  $\hat{O}(\Delta t)^2 = \mathcal{O}(\Delta t)^2$  locally in time and
- when  $\phi = 0.5$ , then this is the (implicit) ‘‘Midpoint’’ scheme, which is stable and  $\hat{O}(\Delta t)^2 = \mathcal{O}(\Delta t)^3$  locally in time.

### 6 Modification of the Time-stepping Scheme for Impact

Consider

$$m_i \dot{\mathbf{v}}_i = \Psi_i^{tot} = \Psi_i^{nf} + \Psi_i^{con} + \Psi_i^{fric} + \Psi_i^{env}. \tag{6.1}$$

Separating the impulsive and continuous forces and applying the trapezoidal  $\phi$ -method leads to

$$\frac{\mathbf{v}_i(t + \Delta t) - \mathbf{v}_i(t)}{\Delta t} = \dot{\mathbf{v}}_i(t + \phi\Delta t) \tag{6.2}$$

and

$$\begin{aligned} \mathbf{v}_i(t + \Delta t) &= \mathbf{v}_i(t) + \frac{1}{m_i} \int_t^{t+\Delta t} \Psi_i^{tot} dt \\ &= \frac{1}{m_i} \left( \int_t^{t+\Delta t} (\Psi_i^{nf} + \Psi_i^{env}) dt + \int_t^{t+\delta t} \Psi_i^{con} dt \right. \\ &\quad \left. + \int_t^{t+\delta t} \Psi_i^{fric} dt \right) \end{aligned}$$

$$\begin{aligned} &\approx \frac{1}{m_i} ((\phi(\Psi_i^{nf}(t + \Delta t) + \Psi_i^{env}(t + \Delta t)) \\ &\quad + (1 - \phi)(\Psi_i^{nf}(t) + \Psi_i^{env}(t)))\Delta t) \\ &\quad + \frac{1}{m_i} (\overline{\Psi}_i^{con}(t^*)\delta t + \overline{\Psi}_i^{fric}(t^*)\delta t), \end{aligned} \tag{6.3}$$

where  $t \leq t^* \leq t + \Delta t$ . The position can be computed via

$$\begin{aligned} \frac{\mathbf{r}_i(t + \Delta t) - \mathbf{r}_i(t)}{\Delta t} &\approx \mathbf{v}_i(t + \phi\Delta t) \\ \implies \mathbf{r}_i(t + \Delta t) &= \mathbf{r}_i(t) + \mathbf{v}_i(t + \phi\Delta t)\Delta t \end{aligned} \tag{6.4}$$

and

$$\begin{aligned} \mathbf{r}_i(t + \Delta t) &= \mathbf{r}_i(t) + \mathbf{v}_i(t + \phi\Delta t)\Delta t \\ &= \mathbf{r}_i(t) + (\phi\mathbf{v}_i(t + \Delta t) + (1 - \phi)\mathbf{v}_i(t))\Delta t. \end{aligned} \tag{6.5}$$

Explicitly, the position can be written as

$$\begin{aligned} \mathbf{r}_i(t + \Delta t) &= \mathbf{r}_i(t) + \mathbf{v}_i(t)\Delta t \\ &\quad + \frac{\phi\Delta t}{m_i} ((\phi(\Psi_i^{nf}(t + \Delta t) + \Psi_i^{env}(t + \Delta t)) \\ &\quad + (1 - \phi)(\Psi_i^{nf}(t) + \Psi_i^{env}(t)))\Delta t) \\ &\quad + \frac{\phi\Delta t}{m_i} (\overline{\Psi}_i^{con}(t^*)\delta t + \overline{\Psi}_i^{fric}(t^*)\delta t). \end{aligned} \tag{6.6}$$

*Remark* Generally, it is advantageous to follow a ‘‘collide and stream’’ philosophy, similar to Lattice-Boltzmann methods,<sup>9</sup> whereby collisions are evaluated at the end or beginning of the time-step (i.e.  $t^* = t$ , updated at the end of the previous time-step). This also mitigates large numbers of iterations within time-steps if implicit schemes ( $0 < \phi$ ) are used. Generally speaking, if a recursive process is *not employed* (an explicit scheme), the iterative error can accumulate rapidly. However, an overkill approach involving very small time steps, smaller than needed to control the discretization error, simply to suppress a nonrecursive process error, is computationally inefficient. Therefore, the objective of the next subsection is to develop a strategy to adaptively adjust, in fact maximize, the choice of the time step size to control the iterative error, while simultaneously staying below a critical time step size needed to control the discretization error. An important related issue is to simultaneously minimize the computational effort involved. The number of times the system is solved, as opposed to time steps, is taken as the measure of computational effort, since within a time

<sup>9</sup>See, for example, Sukop and Thorne [124] for a basic introduction to Lattice-Boltzmann methods.

step, many system re-solves can take place. We now develop an adaptive iterative scheme by following an approach found in various forms in Zohdi [142–157].

### 6.1 Iterative (Implicit) Solution Methods

We write (6.6) in a slightly more streamlined form for particle  $i$

$$\begin{aligned} \mathbf{r}_i^{L+1} &= \mathbf{r}_i^L + \mathbf{v}_i^L \Delta t \\ &+ \frac{\phi \Delta t}{m_i} \left( (\phi(\Psi_i^{nf,L+1} + \Psi_i^{env,L+1}) \right. \\ &+ (1 - \phi)(\Psi_i^{nf,L} + \Psi_i^{env,L})) \Delta t \\ &+ \frac{\phi \Delta t}{m_i} (\overline{\Psi}_i^{con}(t^*)\delta t + \overline{\Psi}_i^{fric}(t^*)\delta t), \end{aligned} \tag{6.7}$$

which leads to a coupled set equations for  $i = 1, 2, \dots, N^p$  particles. The set of equations represented by (6.7) can be solved recursively.

### 6.2 Recursive Solution

Equation (6.7) can be solved recursively by recasting the relation as

$$\mathbf{r}_i^{L+1,K} = \mathcal{G}(\mathbf{r}_i^{L+1,K-1}) + \mathcal{R}_i, \tag{6.8}$$

where  $K = 1, 2, 3, \dots$  is the index of iteration within time step  $L + 1$  and  $\mathcal{R}_i$  is a remainder term that does not depend

on the solution, i.e.

$$\mathcal{R}_i \neq \mathcal{R}_i(\mathbf{r}_1^{L+1}, \mathbf{r}_2^{L+1}, \dots, \mathbf{r}_N^{L+1}). \tag{6.9}$$

The convergence of such a scheme is dependent on the behavior of  $\mathcal{G}$ . Namely, a sufficient condition for convergence is that  $\mathcal{G}$  is a contraction mapping for all  $\mathbf{r}_i^{L+1,K}$ ,  $K = 1, 2, 3, \dots$ . In order to investigate this further, we define the iteration error as

$$\varpi_i^{L+1,K} \stackrel{\text{def}}{=} \mathbf{r}_i^{L+1,K} - \mathbf{r}_i^{L+1}. \tag{6.10}$$

A necessary restriction for convergence is iterative self consistency, i.e. the “exact” (discretized) solution must be represented by the scheme

$$\mathcal{G}(\mathbf{r}_i^{L+1}) + \mathcal{R}_i = \mathbf{r}_i^{L+1}. \tag{6.11}$$

Enforcing this restriction, a sufficient condition for convergence is the existence of a contraction mapping

$$\begin{aligned} \underbrace{\|\mathbf{r}_i^{L+1,K} - \mathbf{r}_i^{L+1}\|}_{\varpi_i^{L+1,K}} &= \|\mathcal{G}(\mathbf{r}_i^{L+1,K-1}) - \mathcal{G}(\mathbf{r}_i^{L+1})\| \\ &\leq \eta^{L+1,K} \|\mathbf{r}_i^{L+1,K-1} - \mathbf{r}_i^{L+1}\|, \end{aligned}$$

where, if  $0 \leq \eta^{L+1,K} < 1$  for each iteration  $K$ , then  $\varpi_i^{L+1,K} \rightarrow \mathbf{0}$  for any arbitrary starting value  $\mathbf{r}_i^{L+1,K=0}$ , as  $K \rightarrow \infty$ . This type of contraction condition is sufficient, but not necessary, for convergence. Explicitly, the recursion is

$$\begin{aligned} \mathbf{r}_i^{L+1,K} &= \underbrace{\mathbf{r}_i^L + \mathbf{v}_i^L \Delta t + \frac{\phi(\Delta t)^2}{m_i} \left( (1 - \phi)(\Psi_i^{nf}(\mathbf{r}^L) + \Psi_i^{env}(\mathbf{r}^L)) \right)}_{\mathcal{R}} \\ &+ \underbrace{\frac{\phi(\Delta t)^2}{m_i} \left( (\phi(\Psi_i^{nf,L+1} + \Psi_i^{env,L+1})) \Delta t + \overline{\Psi}_i^{con}(t^*)\delta t + \overline{\Psi}_i^{fric}(t^*)\delta t \right)}_{\mathcal{G}(\mathbf{r}^{L+1,K-1})}, \end{aligned} \tag{6.12}$$

where

$$\begin{aligned} \Psi_i^{nf \text{ or } env,L} &\stackrel{\text{def}}{=} \Psi_i^{nf \text{ or } env,L}(\mathbf{r}_1^L, \mathbf{r}_2^L, \dots, \mathbf{r}_N^L), \end{aligned} \tag{6.13}$$

and

$$\begin{aligned} \Psi_i^{nf \text{ or } env,L+1,K-1} &\stackrel{\text{def}}{=} \Psi_i^{nf \text{ or } env,L+1,K-1} \\ &\times (\mathbf{r}_1^{L+1,K-1}, \mathbf{r}_2^{L+1,K-1}, \dots, \mathbf{r}_N^{L+1,K-1}). \end{aligned} \tag{6.14}$$

Equation (6.12)’s convergence is scaled by

$$\eta \propto \frac{(\phi \Delta t)^2}{m_i}. \tag{6.15}$$

Therefore, we see that the contraction constant of  $\mathcal{G}$  is (1) directly dependent on the strength of the interaction forces, (2) inversely proportional to  $m$  and (3) directly proportional to  $(\Delta t)^2$  (at time =  $t$ ). Therefore, if convergence is slow within a time step, the time step size, which is adjustable,

can be reduced by an appropriate amount to increase the rate of convergence. Thus, decreasing the time step size improves the convergence, however, we want to simultaneously maximize the time-step sizes to decrease overall computing time, while still meeting an error tolerance on the numerical solution's accuracy. In order to achieve this goal, we follow an approach found in Zohdi [142–157], originally developed for continuum thermo-chemical multifield problems, in which (1) one approximates

$$\eta^{L+1,K} \approx S(\Delta t)^p \quad (6.16)$$

( $S$  is a constant) and (2) one assumes that the error within an iteration to behave according to

$$(S(\Delta t)^p)^K \varpi^{L+1,0} = \varpi^{L+1,K}, \quad (6.17)$$

$K = 1, 2, \dots$ , where  $\varpi^{L+1,0}$  is the initial norm of the iterative error and  $S$  is intrinsic to the system.<sup>10</sup> Our goal is to meet an error tolerance in exactly a preset number of itera-

tions. To this end, one writes

$$(S(\Delta t_{\text{tol}})^p)^{K_d} \varpi^{L+1,0} = \text{TOL}, \quad (6.18)$$

where  $\text{TOL}$  is a tolerance and where  $K_d$  is the number of desired iterations. Typically,  $K_d$  is chosen to be between five to ten iterations. If the error tolerance is not met in the desired number of iterations, the contraction constant  $\eta^{L+1,K}$  is too large. Accordingly, one can solve for a new smaller step size, under the assumption that  $S$  is constant,

$$\Delta t_{\text{tol}} = \Delta t \left( \frac{(\frac{\text{TOL}}{\varpi^{L+1,0}})^{\frac{1}{pK_d}}}{(\frac{\varpi^{L+1,K}}{\varpi^{L+1,0}})^{\frac{1}{pK}}} \right). \quad (6.19)$$

The assumption that  $S$  is constant is not critical, since the time steps are to be recursively refined and unrefined throughout the simulation. Clearly, the expression in (6.19) can also be used for time step enlargement, if convergence is met in less than  $K_d$  iterations. An implementation of the procedure is as follows:

- 
- (1) GLOBAL FIXED-POINT ITERATION : (SET  $i = 1$  AND  $K = 0$ ) :
  - (2) IF  $i > N_p$  THEN GO TO (4)
  - (3) IF  $i \leq N_p$  THEN :
    - (a) COMPUTE POSITION :  $\mathbf{r}_i^{L+1,K}$
    - (b) GO TO (2) FOR NEXT PARTICLE ( $i = i + 1$ )
  - (4) ERROR MEASURE :
    - (a)  $\varpi_K \stackrel{\text{def}}{=} \frac{\sum_{i=1}^{N_p} \|\mathbf{r}_i^{L+1,K} - \mathbf{r}_i^{L+1,K-1}\|}{\sum_{i=1}^{N_p} \|\mathbf{r}_i^{L+1,K} - \mathbf{r}_i^L\|}$  (normalized)
    - (b)  $Z_K \stackrel{\text{def}}{=} \frac{\varpi_K}{\text{TOL}_r}$
    - (c)  $\Phi_K \stackrel{\text{def}}{=} \left( \frac{(\frac{\text{TOL}}{\varpi_0})^{\frac{1}{pK_d}}}{(\frac{\varpi_K}{\varpi_0})^{\frac{1}{pK}}} \right)$
  - (5) IF TOLERANCE MET ( $Z_K \leq 1$ ) AND  $K < K_d$  THEN :
    - (a) INCREMENT TIME :  $t = t + \Delta t$
    - (b) CONSTRUCT NEW TIME STEP :  $\Delta t = \Phi_K \Delta t$ ,
    - (c) SELECT MINIMUM :  $\Delta t = \text{MIN}(\Delta t^{\text{lim}}, \Delta t)$  AND GO TO (1)
  - (6) IF TOLERANCE NOT MET ( $Z_K > 1$ ) AND  $K = K_d$  THEN :
    - (a) CONSTRUCT NEW TIME STEP :  $\Delta t = \Phi_K \Delta t$
    - (b) RESTART AT TIME =  $t$  AND GO TO (1)
- 

<sup>10</sup>For the class of problems under consideration, due to the quadratic dependency on  $\Delta t$ ,  $p \approx 2$ .

Time-step size adaptivity is important, since the system's dynamics and configuration can dramatically change over

the course of time, possibly requiring quite different time step sizes to control the iterative error. However, to maintain the accuracy of the time-stepping scheme, one must respect an upper bound dictated by the discretization error, i.e.,  $\Delta t \leq \Delta t^{lim}$ .

### 7 PART II: Thermal Effects and Coupled Systems

In certain applications, in addition to the near-field and contact effects introduced thus far, thermal behavior is of interest, for example when the particles impact one another vigorously. In many cases, the source of heat generated during impact in such flows can be traced to the reactivity of the particles. This affects the mechanics of impact, for example, due to thermal softening. For instance, the presence of a reactive substance (such as hydrogen gas) adsorbed onto the surface can be a source of additional significant heat generation, through thermochemical reactions activated by impact forces, which thermally softens the material, thus reducing the coefficient of restitution, which in turn strongly affects the mechanical impact event itself (Fig. 4).

To illustrate how one can incorporate thermal effects, a somewhat ad-hoc approach, building on the relation in (4.10), is to construct a thermally dependent coefficient of restitution as follows (multiplicative decomposition)

$$e \stackrel{\text{def}}{=} \left( \max \left( e_o \left( 1 - \frac{\Delta v_n}{v^*} \right), e^- \right) \right) \left( \max \left( \left( 1 - \frac{\theta}{\theta^*} \right), 0 \right) \right), \tag{7.1}$$

where  $\theta^*$  can be considered as a thermal softening temperature. In order to determine the thermal state of the particles, we shall decompose the heat generation and heat transfer processes into two stages: (a) stage 1, describing an extremely short time interval when impact occurs,  $\delta t \ll \Delta t$ ,

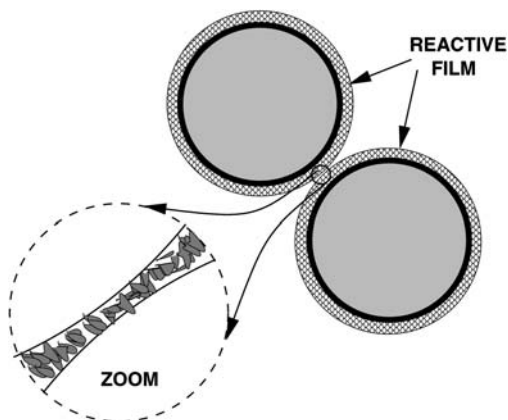


**Fig. 4** Presence of dilute (smaller-scale) reactive gas particles adsorbed onto the surface of two impacting particles (Zohdi [150])

which accounts for the effects of chemical reactions and energy release due to mechanical straining and (b) stage 2, which accounts for the post impact behavior involving heat transfer between particles.

#### 7.1 An Energy Balance

Consistent with the particle-based philosophy, it is assumed that the temperature field is uniform within a particle. We consider an energy balance, governing the interconversions of mechanical, thermal and chemical energy in a system, dictated by the First Law of Thermodynamics. Accordingly, we require the time rate of change of the sum of the kinetic energy ( $\mathcal{K}$ ) and stored energy ( $\mathcal{S}$ ) to be equal to the work rate (power,  $\mathcal{P}$ ), the heat flux due to conduction ( $\mathcal{Q}$ ), the net heat supplied, in this case from two sources, chemical and ( $\mathcal{H}$ ), impact-generated dissipation ( $\mathcal{D}$ ), leading to

$$\frac{d}{dt}(\mathcal{K} + \mathcal{S}) = \mathcal{P} + \mathcal{H} + \mathcal{D} + \mathcal{Q}, \tag{7.2}$$

where the stored energy is comprised of a thermal part,

$$\mathcal{S} = mC\theta, \tag{7.3}$$

where  $C$  is the heat capacity per unit mass and, consistent with our assumptions that the particles deform negligibly during impact, we assume that there is an *insignificant amount of stored mechanical energy*. The kinetic energy is

$$\mathcal{K} = \frac{1}{2}m\mathbf{v} \cdot \mathbf{v}. \tag{7.4}$$

The mechanical power term is due to the forces acting on a particle, namely

$$\mathcal{P} = \frac{d\mathcal{W}}{dt} = \Psi^{tot} \cdot \mathbf{v}, \tag{7.5}$$

and, because

$$\frac{d\mathcal{K}}{dt} = m\dot{\mathbf{v}} \cdot \mathbf{v}, \tag{7.6}$$

and a balance of momentum

$$m\dot{\mathbf{v}} \cdot \mathbf{v} = \Psi^{tot} \cdot \mathbf{v}, \tag{7.7}$$

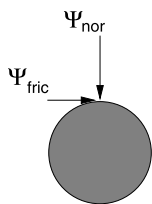
we have

$$\frac{d\mathcal{K}}{dt} = \frac{d\mathcal{W}}{dt} = \mathcal{P}, \tag{7.8}$$

leading to

$$\frac{d\mathcal{S}}{dt} = \mathcal{H} + \mathcal{D} + \mathcal{Q}. \tag{7.9}$$

**Fig. 5** Impulsive forces acting on a particle



One can directly compute the work lost during the impact cycle (compression and recovery, Fig. 2), and hence the dissipation of mechanical energy to be (Fig. 5)

$$\int_t^{t+\delta t} \mathcal{D}_i dt \approx a_1 \bar{I}_n(t) v_n (1 - e^2) \delta t + a_2 \bar{I}_f(t) v_t (1 - e^2) \delta t \stackrel{\text{def}}{=} \bar{\mathcal{D}}_i \delta t, \tag{7.10}$$

where, if  $e = 1$  there is no dissipation,  $e$  being the coefficient of restitution, and where  $0 \leq a_1 \leq 1$  and  $0 \leq a_2 \leq 1$  are dissipation parameters that indicate the proportion of mechanical dissipation that is converted to heat.

### 8 Numerical Scheme

We assume that the dynamics of any (dilute) gas does not affect the motion of the (much heavier) particles.<sup>11</sup> We assume that radiative and convective terms are negligible. We consider only chemical, dissipative and conductive terms. Conduction is a continuous process, while the other two contributions are impulsive in nature, since they owe their existence to impact. Thus,

$$m_i C_i \dot{\theta}_i = \mathcal{F}_i^{\text{tot}} = \mathcal{Q}_i + \mathcal{H}_i + \mathcal{D}_i, \tag{8.1}$$

where  $\mathcal{Q}_i$  represents the conductive contribution from surrounding particles in contact. Separating the impulsive terms and continuous (conduction) term and integrating leads to

$$\frac{\theta_i(t + \Delta t) - \theta_i(t)}{\Delta t} = \dot{\theta}_i(t + \phi \Delta t) \tag{8.2}$$

and

$$\begin{aligned} \theta_i(t + \Delta t) &= \theta_i(t) + \frac{1}{m_i C_i} \int_t^{t+\Delta t} \mathcal{F}_i^{\text{tot}} dt \\ &= \frac{1}{m_i C_i} \left( \int_t^{t+\Delta t} \mathcal{Q}_i dt + \int_t^{t+\delta t} \mathcal{H}_i dt + \int_t^{t+\delta t} \mathcal{D}_i dt \right) \\ &\approx \frac{1}{m_i C_i} \left( (\phi \mathcal{Q}_i(t + \Delta t) + (1 - \phi) \mathcal{Q}_i(t)) \Delta t \right. \\ &\quad \left. + \bar{\mathcal{H}}_i(t^*) \delta t + \bar{\mathcal{D}}_i(t^*) \delta t \right). \end{aligned} \tag{8.3}$$

<sup>11</sup>The gas only supplies a reactive thin film on the particles' surfaces.

### 8.1 Specific Relation for Reactions

The energy released from the reactions is assumed to be proportional to the amount of the surface substance available to be compressed in the contact area between the particles. A typical, ad-hoc approximation in combustion processes is to write, for example,

$$\int_t^{t+\delta t} \mathcal{H}_i dt \approx \left( \kappa \min\left(\frac{|\bar{I}_n|}{I_n^*}, 1\right) \pi b^2 \right) \delta t, \tag{8.4}$$

where  $\bar{I}_n$  is the normal impact force,  $\kappa$  is a reaction (saturation) constant, energy per unit area,  $I_n^*$  is a normalization parameter and  $b$  is the particle radius. For details, for example, see Schmidt [121]. For the grain sizes and material properties of interest, the term in (8.3),  $\frac{\delta \mathcal{H}}{mC}$ , indicates that values of approximately  $\kappa \approx 10^6$  J/m<sup>2</sup> will generate significant amounts of heat.<sup>12</sup> Clearly, these equations are coupled to those of impact through the coefficient of restitution and the velocity-dependent impulse. Additionally, the post-collision velocities are computed from the momentum relations which are coupled to the temperature. Later in the analysis, this equation is incorporated into an overall staggered fixed-point iteration scheme, whereby the temperature is predicted for a given velocity field, and then the velocities are recomputed with the new temperature field, etc. The process is repeated until the fields change negligibly between successive iterations. The entire set of equations is embedded within a larger system, involving the particle dynamics, later in the analysis, and is solved in a recursive, staggered, manner.

### 8.2 Specific Relation for Conduction

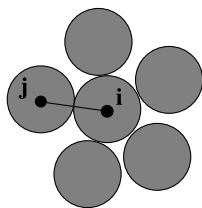
It is assumed that the temperature fields are uniform within the (small) particles. We remark that the validity of using a lumped thermal model, i.e. ignoring temperature gradients and assuming a uniform temperature within a particle, is dictated by the magnitude of the Biot number. A small Biot number indicates that such an approximation is reasonable. The Biot number for spheres scales with the ratio of the particle volume ( $V$ ) to the particle surface area ( $a_s$ ),  $\frac{V}{a_s} = \frac{b}{3}$ , which indicates that a uniform temperature distribution is appropriate, since the particles, by definition, are small. In continuous models of conduction, Fourier's Law leads to

$$\mathcal{Q}_i = \mathbb{K}_i \nabla^2 \theta_i, \tag{8.5}$$

which can be interpreted as the value of the temperature of the node subtracted from the surrounding nodes' tem-

<sup>12</sup>By construction, this model has increased heat production, via  $\delta \mathcal{H}$ , for increasing  $\kappa$ .

**Fig. 6** Conduction between particles



peratures, where  $\mathbb{K}_i$  is the effective particle conductivity. For example, for a three dimensional finite-difference stencil commonly used in numerical methods, we have

$$\begin{aligned}
 Q_i &= \mathbb{K}_i \nabla^2 \theta_i \\
 &\approx \mathbb{K}_i \left( \frac{\theta(x + \Delta x, y, z) - 2\theta(x, y, z) + \theta(x - \Delta x, y, z)}{(\Delta x)^2} \right. \\
 &\quad + \frac{\theta(x, y + \Delta y, z) - 2\theta(x, y, z) + \theta(x, y - \Delta y, z)}{(\Delta y)^2} \\
 &\quad \left. + \frac{\theta(x, y, z + \Delta z) - 2\theta(x, y, z) + \theta(x, y, z - \Delta z)}{(\Delta z)^2} \right), \tag{8.6}
 \end{aligned}$$

which can be generalized

$$Q_i = \mathbb{K}_i \sum_{j=1}^{N_c} \frac{(\theta_j - \theta_i)}{\|\mathbf{r}_j - \mathbf{r}_i\|^2}, \tag{8.7}$$

where the summation extends overall particles  $j = 1, 2, 3, \dots, N_c$  that are in contact with particle  $i$  (Fig. 6).

The time-stepping formula has the following form

$$\begin{aligned}
 \theta_i(t + \Delta t) &= \theta_i(t) + \frac{\delta t}{m_i C_i} (\overline{\mathcal{H}}_i + \overline{\mathcal{D}}_i) \\
 &\quad + \frac{\Delta t}{m_i C_i} \left( \phi \mathbb{K}_i \sum_{j=1}^{N_c} \frac{\theta_j(t + \Delta t) - \theta_i(t + \Delta t)}{\|\mathbf{r}_j(t + \Delta t) - \mathbf{r}_i(t + \Delta t)\|^2} \right) \\
 &\quad + \frac{\Delta t}{m_i C_i} \left( (1 - \phi) \mathbb{K}_i \sum_{j=1}^{N_c} \frac{\theta_j(t) - \theta_i(t)}{\|\mathbf{r}_j(t) - \mathbf{r}_i(t)\|^2} \right) \tag{8.8}
 \end{aligned}$$

which can be rewritten as

$$\begin{aligned}
 \theta_i(t + \Delta t) &= A \theta_i(t) + \frac{A \delta t}{m_i C_i} (\overline{\mathcal{H}}_i + \overline{\mathcal{D}}_i) \\
 &\quad + \frac{A \Delta t}{m_i C_i} \left( \phi \mathbb{K}_i \sum_{j=1}^{N_c} \frac{\theta_j(t + \Delta t)}{\|\mathbf{r}_j(t + \Delta t) - \mathbf{r}_i(t + \Delta t)\|^2} \right) \\
 &\quad + \frac{A \Delta t}{m_i C_i} \left( (1 - \phi) \mathbb{K}_i \sum_{j=1}^{N_c} \frac{\theta_j(t) - \theta_i(t)}{\|\mathbf{r}_j(t) - \mathbf{r}_i(t)\|^2} \right), \tag{8.9}
 \end{aligned}$$

where

$$A = \left( 1 + \frac{\phi \mathbb{K}_i \Delta t}{m_i C_i} \sum_{j=1}^{N_c} \frac{1}{\|\mathbf{r}_j(t + \Delta t) - \mathbf{r}_i(t + \Delta t)\|^2} \right)^{-1}. \tag{8.10}$$

An iterative scheme can be set up  $K = 1, 2, 3, \dots$ ,

$$\begin{aligned}
 \theta_i^{K+1}(t + \Delta t) &= A^K \theta_i(t) + \frac{A^K \delta t}{m_i C_i} (\overline{\mathcal{H}}_i^K + \overline{\mathcal{D}}_i^K) \\
 &\quad + \frac{A^K \Delta t}{m_i C_i} \left( \phi \mathbb{K}_i \sum_{j=1}^{N_c} \frac{\theta_j^K(t + \Delta t)}{\|\mathbf{r}_j^K(t + \Delta t) - \mathbf{r}_i^K(t + \Delta t)\|^2} \right) \\
 &\quad + \frac{A^K \Delta t}{m_i C_i} \left( (1 - \phi) \mathbb{K}_i \sum_{j=1}^{N_c} \frac{\theta_j(t) - \theta_i(t)}{\|\mathbf{r}_j(t) - \mathbf{r}_i(t)\|^2} \right). \tag{8.11}
 \end{aligned}$$

We note that (8.11) is of the general form:

$$\theta(t + \Delta t) = \mathcal{G}(\theta(t + \Delta t)) + \mathcal{R}, \tag{8.12}$$

where  $\mathcal{R} \neq \mathcal{R}(\theta(t + \Delta t))$ , and where  $\mathcal{G}$ 's behavior is controlled by the magnitude of  $\Delta t$ . Clearly, the temperature is coupled to the mechanical behavior of the system. Next, we develop a multiphysical staggering scheme to solve the overall system.

### 9 Multiphysical Staggering Scheme

Broadly speaking, staggering schemes proceed by solving each field equation individually, allowing only the primary field variable to be active. After the solution of each field equation, the primary field variable is updated, and the next field equation is addressed in a similar manner. Such approaches have a long history in the computational mechanics community. For example, see Park and Felippa [108], Zienkiewicz [139], Zienkiewicz et al. [140], Schrefler [122], Tursa and Schrefler [133], Lewis et al. [80], Doltsinis [20, 21], Piperno [110], Lewis and Schrefler [79], Armero and Simo [4–6], Armero [7], Le Tallec and Mouro [78], Zohdi [142–157] and the extensive works of Farhat and coworkers (Piperno et al. [111], Farhat et al. [29], Lesoinne and Farhat [77], Farhat and Lesoinne [30], Piperno et al. [111], Piperno and Farhat [112] and Farhat et al. [31]). For recent work involving staggering schemes for piezoelectric applications, see Fish and Chen [32]. Also, for a review of the state of the art, see Michopoulos et al. [92]. Generally speaking, if a recursive staggering process is *not employed* (an explicit coupling scheme), the staggering error can accumulate rapidly. However, an overkill approach (involving

very small time steps, smaller than needed to control the discretization error), simply to suppress a nonrecursive staggering process error, is computationally inefficient. Therefore, the objective of the next subsection is to develop a strategy to adaptively adjust, in fact maximize, the choice of the time step size in order to control the staggering error, while simultaneously staying below a critical time step size needed to control the discretization error (as stated before). An important related issue is to simultaneously minimize the computational effort involved. The number of times the multifield system is solved, as opposed to time steps, is taken as the measure of computational effort since, within a time step, many multifield system re-solves can take place. We now further develop the staggering scheme introduced earlier by extending an approach found in Zohdi [142–157].

### 9.1 A General Iterative Framework

We consider an abstract setting, whereby one solves for the particle positions, assuming the thermal fields fixed,

$$\mathcal{A}_1(\underline{\mathbf{r}}^{L+1,K}, \theta^{L+1,K-1}) = \mathcal{F}_1(\mathbf{r}^{L+1,K-1}, \theta^{L+1,K-1}), \quad (9.1)$$

then one solves for the thermal fields, assuming the particle positions fixed,

$$\mathcal{A}_2(\mathbf{r}^{L+1,K}, \underline{\theta}^{L+1,K}) = \mathcal{F}_2(\mathbf{r}^{L+1,K}, \theta^{L+1,K-1}), \quad (9.2)$$

where the only underlined variable is “active”,  $L$  indicates the time step and  $K$  indicates the iteration counter. Within the staggering scheme, implicit time-stepping methods, with time step size adaptivity, will be used throughout the upcoming analysis.

Continuing where (6.18) left off, we define the normalized errors within each time step, for the two fields,

$$\begin{aligned} \varpi_{rK} &\stackrel{\text{def}}{=} \frac{\|\mathbf{r}^{L+1,K} - \mathbf{r}^{L+1,K-1}\|}{\|\mathbf{r}^{L+1,K} - \mathbf{r}^L\|} \quad \text{and} \\ \varpi_{\theta K} &\stackrel{\text{def}}{=} \frac{\|\theta^{L+1,K} - \theta^{L+1,K-1}\|}{\|\theta^{L+1,K} - \theta^L\|}. \end{aligned} \quad (9.3)$$

We define maximum “violation ratio”, i.e. as the larger of the ratios of each field variable’s error to its corresponding tolerance, by  $Z_K \stackrel{\text{def}}{=} \max(z_{rK}, z_{\theta K})$ , where

$$z_{rK} \stackrel{\text{def}}{=} \frac{\varpi_{rK}}{TOL_r} \quad \text{and} \quad z_{\theta K} \stackrel{\text{def}}{=} \frac{\varpi_{\theta K}}{TOL_\theta}, \quad (9.4)$$

with the minimum scaling factor defined as  $\Phi_K \stackrel{\text{def}}{=} \min(\phi_{rK}, \phi_{\theta K})$ , where

$$\phi_{rK} \stackrel{\text{def}}{=} \left( \frac{(\frac{TOL_r}{\varpi_{r0}})^{\frac{1}{pK_d}}}{(\frac{\varpi_{rK}}{\varpi_{r0}})^{\frac{1}{pK}}} \right), \quad \phi_{\theta K} \stackrel{\text{def}}{=} \left( \frac{(\frac{TOL_\theta}{\varpi_{\theta0}})^{\frac{1}{pK_d}}}{(\frac{\varpi_{\theta K}}{\varpi_{\theta0}})^{\frac{1}{pK}}} \right). \quad (9.5)$$

The algorithm is as follows:

- 
- (1) GLOBAL FIXED-POINT ITERATION : (SET  $i = 1$  AND  $K = 0$ ) :
  - (2) IF  $i > N_p$  THEN GO TO (4)
  - (3) IF  $i \leq N_p$  THEN : (FOR PARTICLE  $i$ )
    - (a) COMPUTE POSITION :  $\mathbf{r}_i^{L+1,K}$
    - (b) COMPUTE TEMPERATURE :  $\theta_i^{L+1,K}$
    - (c) GO TO (2) AND NEXT PARTICLE ( $i = i + 1$ )
  - (4) ERROR MEASURES (normalized) :
    - (a)  $\varpi_{rK} \stackrel{\text{def}}{=} \frac{\sum_{i=1}^{N_p} \|\mathbf{r}_i^{L+1,K} - \mathbf{r}_i^{L+1,K-1}\|}{\sum_{i=1}^{N_p} \|\mathbf{r}_i^{L+1,K} - \mathbf{r}_i^L\|}, \quad \varpi_{\theta K} \stackrel{\text{def}}{=} \frac{\sum_{i=1}^{N_p} \|\theta_i^{L+1,K} - \theta_i^{L+1,K-1}\|}{\sum_{i=1}^{N_p} \|\theta_i^{L+1,K} - \theta_i^L\|}$
    - (b)  $Z_K \stackrel{\text{def}}{=} \max(z_{rK}, z_{\theta K})$  where  $z_{rK} \stackrel{\text{def}}{=} \frac{\varpi_{rK}}{TOL_r}, \quad z_{\theta K} \stackrel{\text{def}}{=} \frac{\varpi_{\theta K}}{TOL_\theta}$
    - (c)  $\Phi_K \stackrel{\text{def}}{=} \min(\phi_{rK}, \phi_{\theta K})$  where  $\phi_{rK} \stackrel{\text{def}}{=} \left( \frac{(\frac{TOL_r}{\varpi_{r0}})^{\frac{1}{pK_d}}}{(\frac{\varpi_{rK}}{\varpi_{r0}})^{\frac{1}{pK}}} \right), \quad \phi_{\theta K} \stackrel{\text{def}}{=} \left( \frac{(\frac{TOL_\theta}{\varpi_{\theta0}})^{\frac{1}{pK_d}}}{(\frac{\varpi_{\theta K}}{\varpi_{\theta0}})^{\frac{1}{pK}}} \right)$
  - (5) IF TOLERANCE MET ( $Z_K \leq 1$ ) AND  $K < K_d$  THEN :
    - (a) INCREMENT TIME :  $t = t + \Delta t$
    - (b) CONSTRUCT NEW TIME STEP :  $\Delta t = \Phi_K \Delta t$ ,
    - (c) SELECT MINIMUM :  $\Delta t = \text{MIN}(\Delta t^{lim}, \Delta t)$  AND GO TO (1)
  - (6) IF TOLERANCE NOT MET ( $Z_K > 1$ ) AND  $K = K_d$  THEN :
    - (a) CONSTRUCT NEW TIME STEP :  $\Delta t = \Phi_K \Delta t$
    - (b) RESTART AT TIME =  $t$  AND GO TO (1)

The overall goal is to deliver solutions where staggering (incomplete coupling) error is controlled and the temporal discretization accuracy dictates the upper limits on the time step size ( $\Delta t^{lim}$ ).

*Remark* A significant speed up in the computation can be achieved via Sorting and Binning (SB) methods. SB methods proceed by partitioning the whole domain into bins. The particles are sorted by the bins in which they reside. The particle interaction proceeds, bin by bin, where the particles within a bin potentially only interact with particles in other nearest neighbor bins. Essentially, for a given particle in a bin, contact searches and near-field interaction search are conducted with particles in the neighboring bins only. The approach is relatively straightforward to implement and can speed up the computation dramatically. In order to determine the approximate savings, let us denote the number of particles by  $N_p$ . The computational costs are as follows:

- To determine (sort) which particle belong to which bins:  $\mathcal{O}(N_p)$ .
- For a bin, for each particle in the bin, search over only the particles in the neighboring bins. For example, consider an evenly distributed set of particles on Fig. 7. Denote the number of bins by  $N_b$ , and the number of nearest-neighbor bins by  $N_{nn}$ . The total cost for searching (to compute the particle interactions) and sweeping through all of the bins, is

$$\left(\frac{N_p}{N_b}\right) \left(N_{nn} \left(\frac{N_p}{N_b}\right)\right) N_b = N_p^2 \left(\frac{N_{nn}}{N_b}\right). \tag{9.7}$$

For example for an *immediate nearest neighbor* list,  $N_{nn} = 27$  (in 3-D, including the central bin).

*Note 1:* One can reduce computation by accounting for particle-particle interaction that has been computed already from previous bin computation,  $i - j$  interaction, when computing  $j - i$  interaction.

*Note 2:* One can assume that particles stay in the bins for a few time steps, and that one does not need to resort immediately. One can construct so-called “interaction” or “Verlet” lists of neighboring particles which particles interact

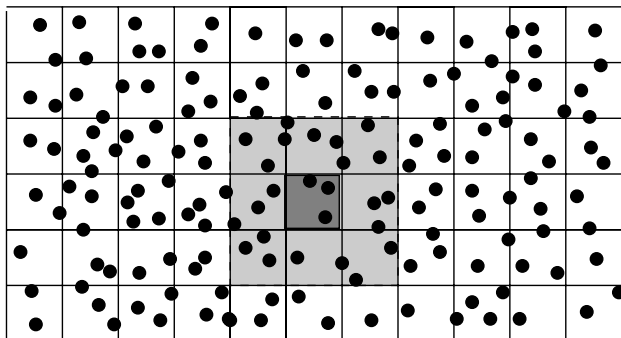


Fig. 7 Binning of the particles in a flow

with, for a few time steps, and then update the interaction periodically (see Pöschel and Schwager [113]).

One can also employ the following complementary techniques:

- *Domain decomposition:* involve methods where domain is partitioned into subdomains, and the particles within each domain are sent to a processor and stepped forward in time, but with the positions of the particles outside of the subdomain fixed (relative to the particles in that subdomain). This is done for all of the domains separately, then the positions of all of the particles are updated and this information is shared between processors, then the process is repeated.
- *Fast (summation) multipole techniques:* involve methods to compute far-field interaction rapidly by exploiting the separable (near and far field) structure of multipole interaction.

The above techniques were not implemented here, however they are relatively easy to employ.

### 10 External EM-fields: Two-scale Macro-field/Near-field Decomposition

Now consider the dynamics of these particles are governed by

$$m_i \ddot{\mathbf{r}}_i = \Psi_i^{tot}(\mathbf{r}_1, \mathbf{r}_2, \dots, \mathbf{r}_{N_p}) = \Psi_i^{nf} + \Psi_i^{con} + \Psi_i^{fric} + \underbrace{q_i(\mathbf{E}^{ext} + \mathbf{v}_i \times \mathbf{B}^{ext})}_{\Psi_i^{env}}, \tag{10.1}$$

$\mathbf{r}_i$  is the position vector of the  $i$ th particle  $\Psi_i^{tot}$  represents all forces acting on particle  $i$ ,  $\Psi_i^{nf}$  represents near-field forces acting on particle  $i$ ,  $\Psi_i^{con}$  represents contact forces acting on particle  $i$ ,  $\Psi_i^{fric}$  represents friction forces acting on particle  $i$  and where the fields:  $\Psi_i^{env} = q_i(\mathbf{E}^{ext} + \mathbf{v}_i \times \mathbf{B}^{ext})$ , are *externally controlled*. The presence of the Lorentz force can cause helical-type motion to occur, which will be discussed later.

## 11 Model Problems

### 11.1 Initial Configurations: Preprocessing

In order to generate an initial particle configuration one typically uses a classical Random Sequential Addition algorithm of Widom [135], which places nonoverlapping particles randomly into the domain of interest. However, the RSA algorithm usually cannot achieve extremely high density (volume fraction) configurations. For high-density sprays, the well-known, equilibrium-driven, Metropolis algorithm is

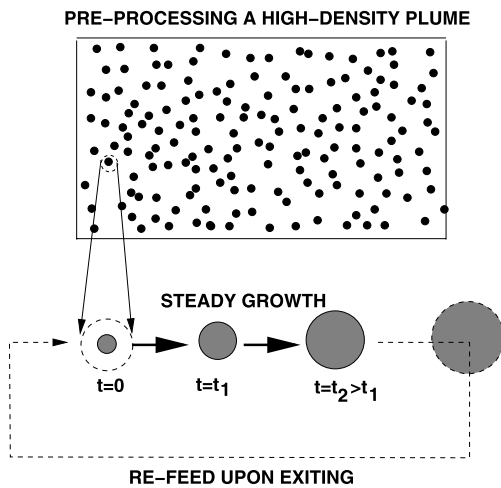


**Fig. 8** Growth schemes

widely used. However, for extremely high volume fractions, effectively packing (and “jamming”) particles together, a relatively new class of methods, based on simultaneous particle flow and growth, has been developed by Torquato and coworkers (Torquato [132], Kansaal et al. [67] and Donev et al. [22–24]), which are computationally efficient and straightforward to implement (Fig. 8).

The algorithm proceeds by allowing the particles to “grow” in the flow as the particles are moving, thus permitting the particles to slightly “bump” and rearrange themselves through momentum exchange. The growth rate is selected to be very gradual. For example, before a jet of particles is ready for an impact simulation, one can employ periodic boundary conditions (where the exiting particles are “re-fed” into the system), and at the end of each time step in this preliminary simulation, one can adjust the radius of the  $i$ th particle via

$$r_i(t + \Delta t) = r_i(t = 0) \left( 1 + \mathcal{L} \frac{t}{T} \right), \quad (11.1)$$

where  $\mathcal{L}$  is a user selected growth rate,  $T$  is the total simulation “growth time”. When the volume fraction has reached a sufficiently high level (this is determined by selecting  $\mathcal{L}$  and  $T$ ), the jet may then be used for the impact simulation with an external object.

## 11.2 Numerical Examples

We consider a model problem of a particulate jet impinging onto a (1) neutral surface and (2) an electromagnetic “wall”, placed before the surface (Fig. 9). The absolute dimensions are unimportant for the model problem, and have been normalized.<sup>13</sup> We considered a group of  $N_p$  randomly

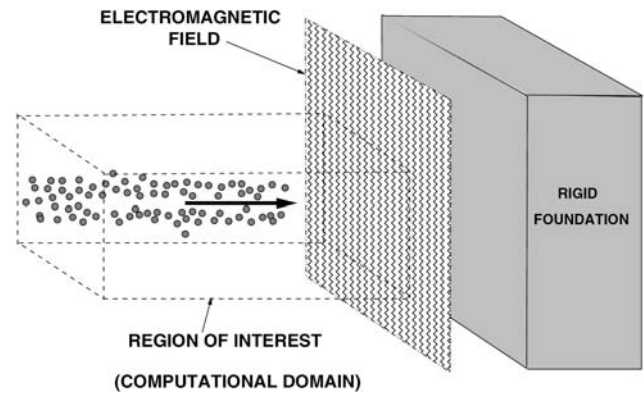


**Fig. 9** A model problem: a particulate jet-spray impinging onto a (1) neutral surface, and (2) an electromagnetic “wall”

positioned particles in a jet-spray domain with dimensions  $L_1 = 20 \times L_2 = 0.75 \times L_3 = 0.75$  meters (m). The initial particle radius (monodisperse) was  $r = 0.05$  m and pre-processed (“grown”, without near-field neutral collisions) to  $r = 0.1$  m, with the previously mentioned steady growth algorithm; which was then used for the simulations. The relevant simulation parameters were:

- number of particles = 1500, with  $\alpha_{ij} = \bar{\alpha}_{ij} q_i q_j c_i c_j$  and  $c_i = \pm 1$  (positive/negative),  $q_i = q_j = 1$ ,
- $\bar{\alpha}_{ij1} = 2, \bar{\alpha}_{ij2} = 1, \beta_{ij1} = 1, \beta_{ij2} = 2$ ,
- mass density of the particles =  $2000 \text{ kg/m}^3$ ,
- initial velocity =  $(30, 0, 0) \text{ m/s}$ ,
- initial mean position =  $(-5, 0, 0) \text{ m}$ ,
- coefficient of dynamic friction,  $\mu_d = 0.1$ ,
- coefficient of static friction,  $\mu_s = 0.2$ ,
- baseline coefficient of restitution,  $e_o = 0.5$ ,
- limit of coefficient of restitution,  $e^- = 0.2$ ,
- reaction constant,  $\kappa = 10^4 \text{ J/m}^2$ ,
- thermal (reference temperature) constant,  $\theta^* = 3000 \text{ K}$ ,
- velocity parameter,  $v^* = 10 \text{ m/s}$ ,
- impact parameter,  $I^* = 1000 \text{ N}$ ,
- conductivity,  $\mathbb{K}_i = 100 \text{ Jm}^2/\text{kg}$ ,
- $\theta(t = 0) = 300 \text{ K}$ ,
- heat capacity,  $C = 10^3 \text{ J/kg K}$ ,
- impulse-thermal conversion,  $a_1 = 1, a_2 = 1$ ,
- target number of fixed point iterations,  $K_d = 6$ ,
- the time-stepping parameter,  $\phi = 0.5$ ,
- $\mathbf{E}^{ext} = (0, 0, 0) \text{ N/coulomb}$ ,
- $\mathbf{B}^{ext} = (0, 0, 1000) \text{ kg/s coulomb}$ ,
- domain bin-grid (rectangular) =  $(70 \times 40 \times 40)$ ,
- simulation duration = 1 second,
- initial time step size = 0.001 seconds,
- time step upper bound = 0.0025 seconds,
- tolerance for the fixed-point iteration =  $10^{-3}$ .

specific system of interest. In other words, the length-scale is essentially irrelevant to the model problem framework.

<sup>13</sup>The transverse dimensions of the jet were set to be approximately unity, initially. All system parameters can be scaled to describe any

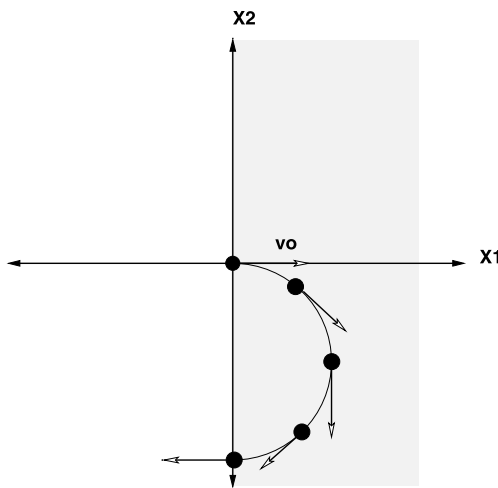


Fig. 10 Trajectory of the particle encountering a B-field

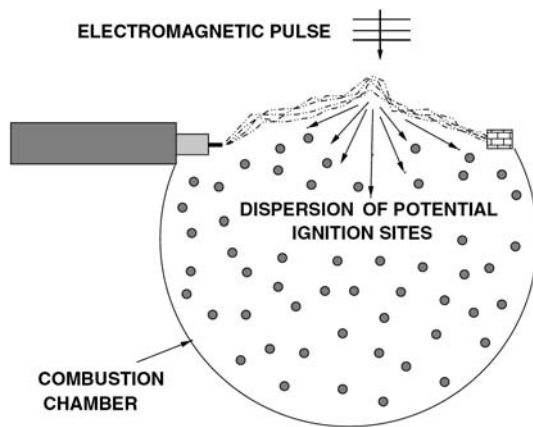


Fig. 11 A spark comprised of a charged ion jet and a possible ablation scheme, with a user-controlled electromagnetic field

Particles that strayed outside of a computational  $4\text{ m} \times 4\text{ m}$  window were thrown out of the computations. We have the following observations:

- Figures 12, 13 and 14 illustrate the evolution of the microstructure of a jet-spray: (1) inter-particle collisions and heating (2) agglomeration and (3) impact with the surface or electromagnetic “wall”.
- Depending on the time allowed for the jet-spray to impact the obstacle, there may not be enough time for clustering to fully evolve. We note that one can break up large detrimental clusters with B-fields by separating positive and negative charge clusters that have bonded together. In the case considered, the electromagnetic field is strong enough to repel the particulates. We remark that several different scenarios could be considered by varying the initial kinetic energy of the jet, for example, (1) epitaxy (particle lay-up) and (2) particle embedding/infiltration into the wall. Also, depending on the external fields, for ex-

ample in the vicinity of the surface, a pure E-field will draw in either positive or negative charged particles (thus separating them), although in this particular example, the E-field was set to zero.

- The key signature of the onset of agglomeration/clustering is the sudden spike in the impact force over time (Figs. 15–17), as opposed to the force “signature” produced by a steady stream of particles, which is more or less constant.
- The system achieves a much greater temperature in the case of the neutral wall (Fig. 20), due to the particle impact against the wall.
- One can compute the discrete “vortex” (angular momentum about the mass center) of the system:

$$\mathbf{V} \stackrel{\text{def}}{=} \frac{1}{\mathcal{M}} \sum_{i=1}^{N_p} m_i (\mathbf{r}_i - \mathbf{r}_{cm}) \times (\mathbf{v}_i - \mathbf{v}_{cm}), \quad (11.2)$$

where  $\mathcal{M} = \sum_{i=1}^{N_p} m_i$  is the total system mass

$$\mathbf{r}_{cm} \stackrel{\text{def}}{=} \frac{1}{\mathcal{M}} \sum_{i=1}^{N_p} m_i \mathbf{r}_i \quad (11.3)$$

and

$$\mathbf{v}_{cm} \stackrel{\text{def}}{=} \frac{1}{\mathcal{M}} \sum_{i=1}^{N_p} m_i \mathbf{v}_i. \quad (11.4)$$

The discrete vortex is an indication of the spinning of the particles, relative to the system center of mass. In the case of having an electromagnetic wall present, the vortex is significantly higher (Fig. 18, see also Fig. 19 for Cg motion). *This is due to the Lorentz force.* In order to understand this effect, consider the motion of a single particle with an initially constant velocity, moving into a domain with a static electromagnetic field (Fig. 10), which will experience a torque and acceleration. The equation of motion is, with  $\mathbf{E}^{ext} = (E_1^{ext}, E_2^{ext}, E_3^{ext})$  and  $\mathbf{B}^{ext} = (B_1^{ext}, B_2^{ext}, B_3^{ext})$ ,

$$m \dot{\mathbf{v}} = q(\mathbf{E}^{ext} + \mathbf{v} \times \mathbf{B}^{ext}), \quad (11.5)$$

or explicitly

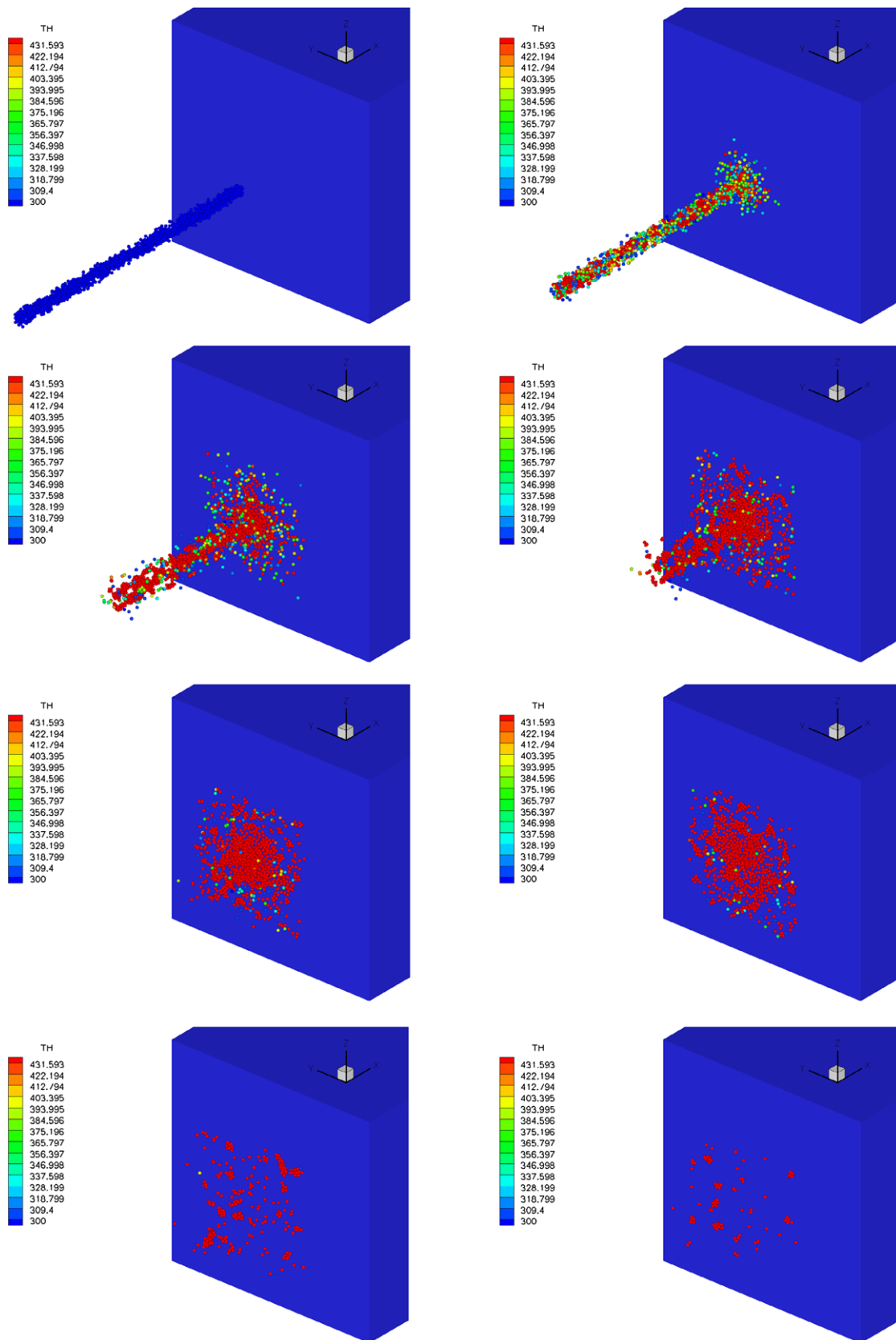
$$\dot{v}_1 = \frac{q}{m} (E_1^{ext} + (v_2 B_3^{ext} - v_3 B_2^{ext})), \quad (11.6)$$

and

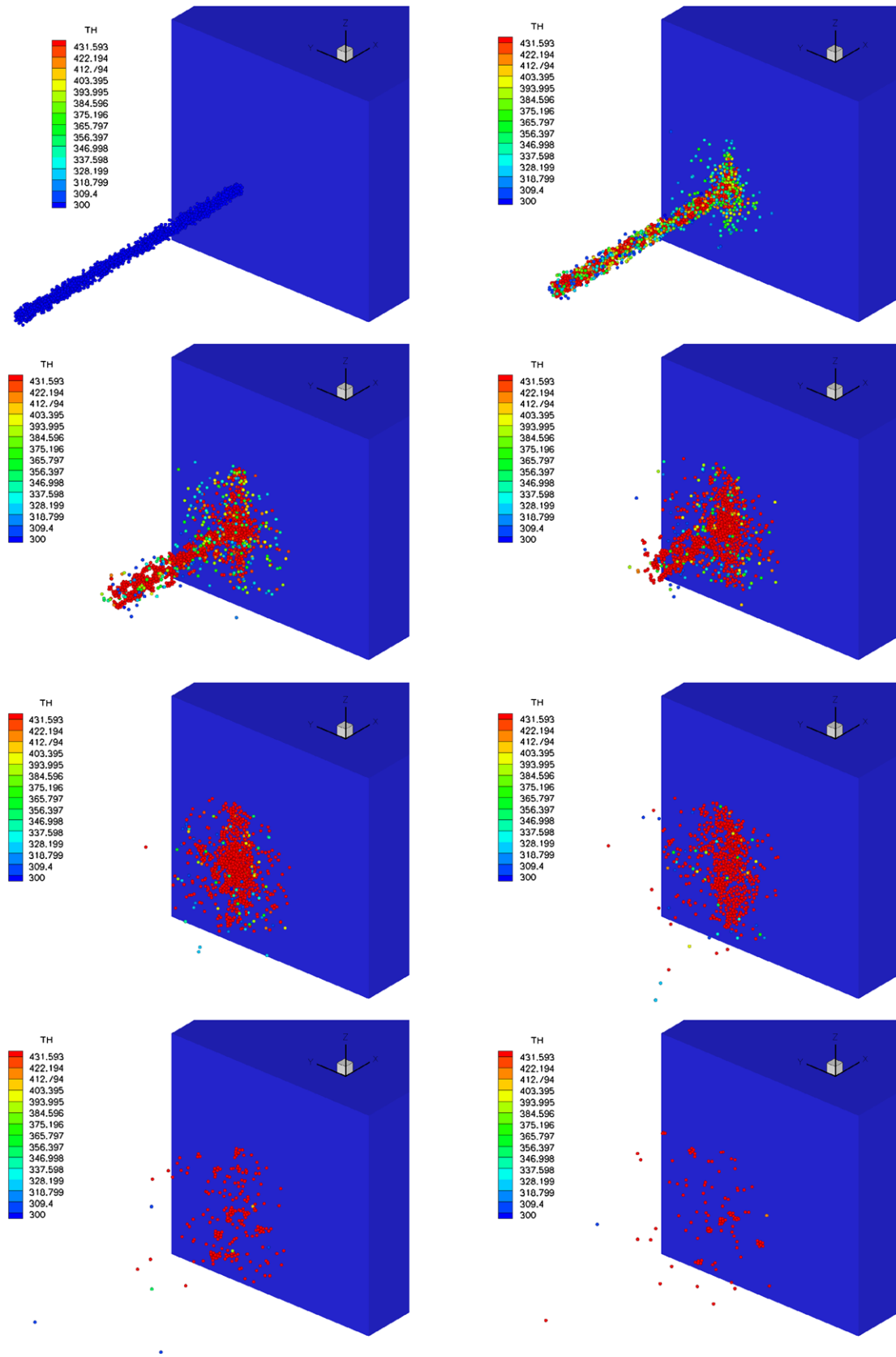
$$\dot{v}_2 = \frac{q}{m} (E_2^{ext} - (v_1 B_3^{ext} - v_3 B_1^{ext})), \quad (11.7)$$

and

$$\dot{v}_3 = \frac{q}{m} (E_3^{ext} + (v_1 B_2^{ext} - v_2 B_1^{ext})). \quad (11.8)$$

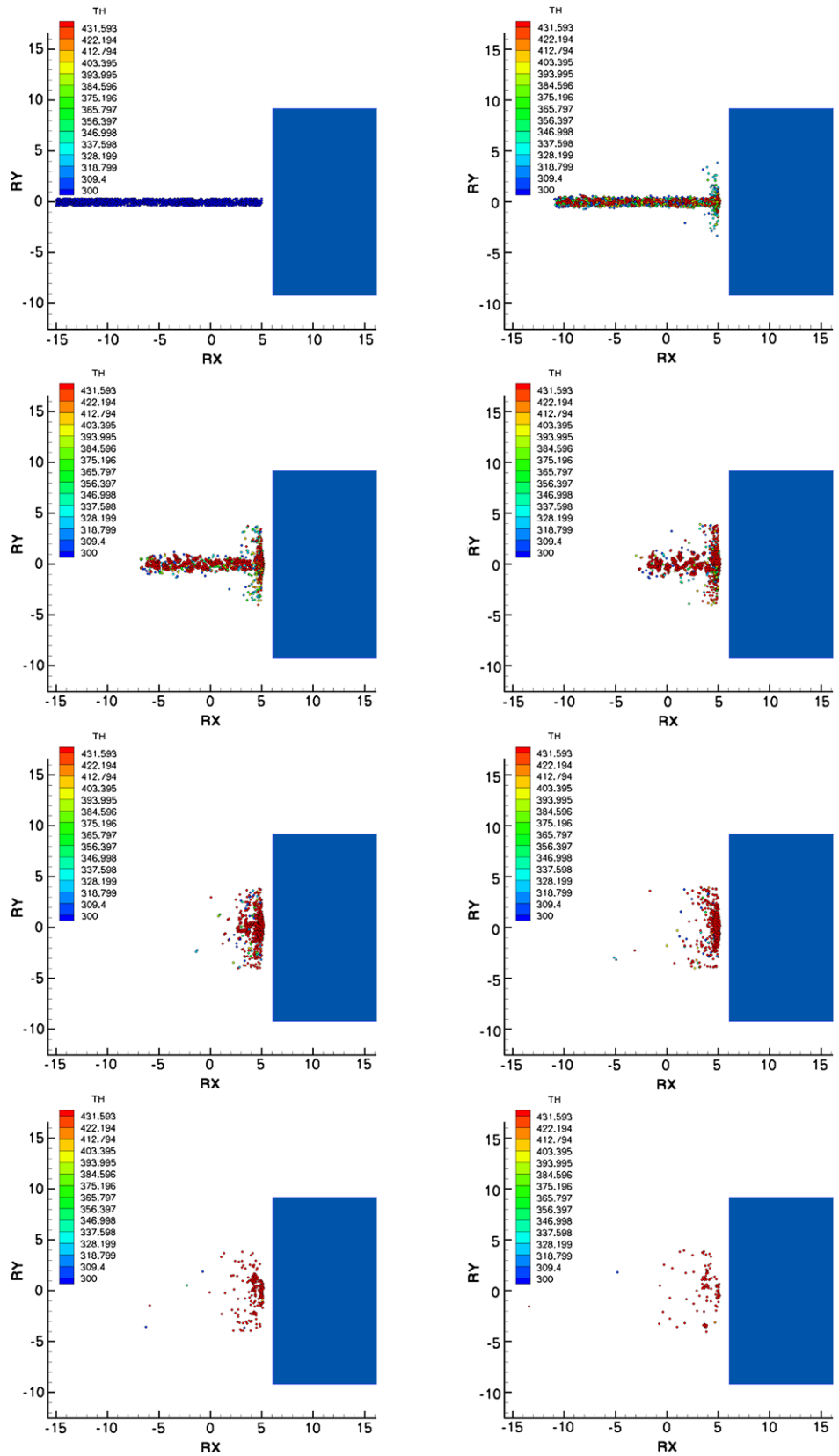


**Fig. 12** Top to bottom and left to right: impact of a charged jet against an immovable obstacle. Note that only particles that are in the domain of interest are shown



**Fig. 13** Top to bottom and left to right: impact of a charged jet against an electromagnetic field ahead of an immovable obstacle. Note that only particles that are in the domain of interest are shown

**Fig. 14** *Top to bottom and left to right (SIDE VIEW): impact of a charged jet against an electromagnetic field ahead of an immovable obstacle. Note that only particles that are in the domain of interest are shown*



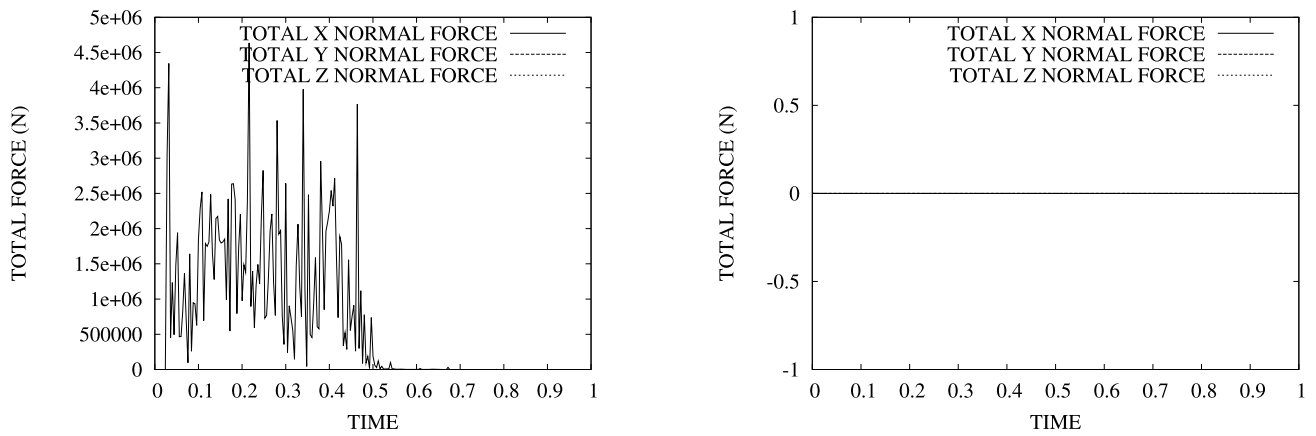


**Fig. 15** All forces acting on the obstacle. *Left*: charged and *Right*: charged with a field. No contact is made when the electromagnetic field is present. Note that only particles that are in the domain of interest are included in the computations

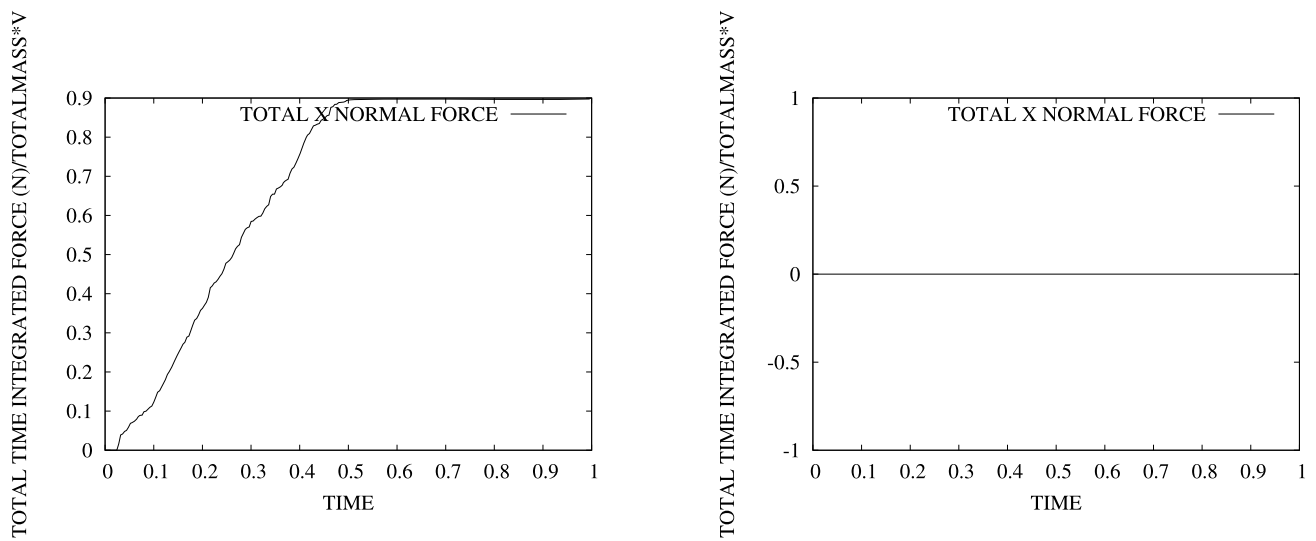


**Fig. 16** The integrated impulses  $\int_0^T \mathbf{I} dt$  maximum force. *Left*: charged. *Right*: charged with field. Note that only particles that are in the domain of interest are included in the computations

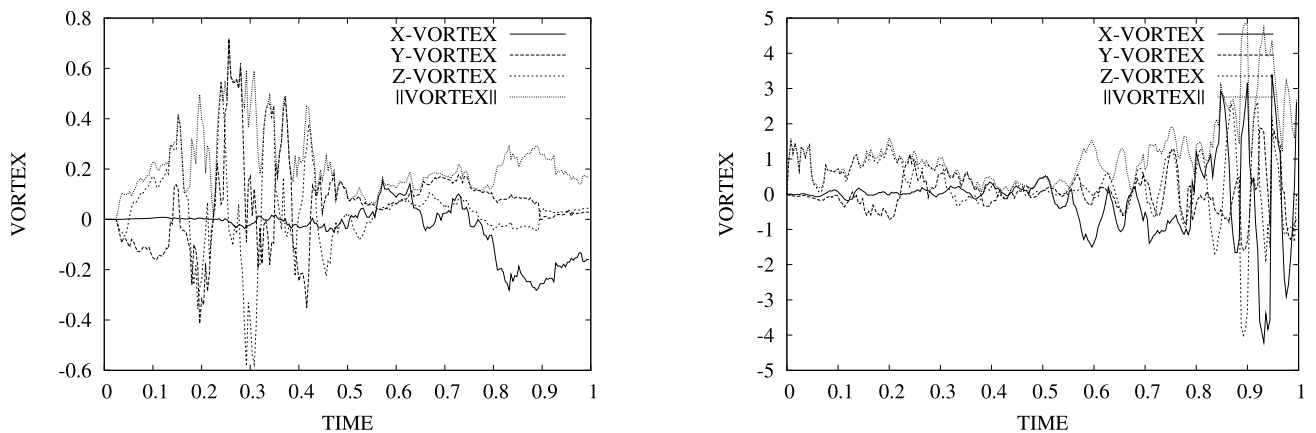


**Fig. 17** The total vortex. *Left*: charged. *Right*: charged with field. The Lorentz force induces a large amount of spin within the system, relative to the case where no electromagnetic field present. Note that only particles that are in the domain of interest are included in the computations

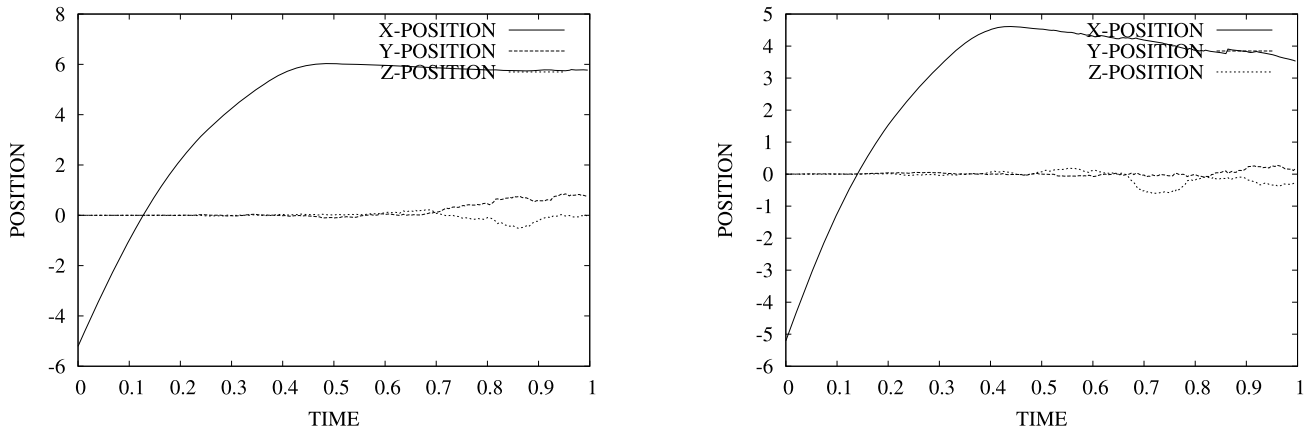


**Fig. 18** The CG-position. *Left*: charged. *Right*: charged with field. Note that only particles that are in the domain of interest are included in the computations

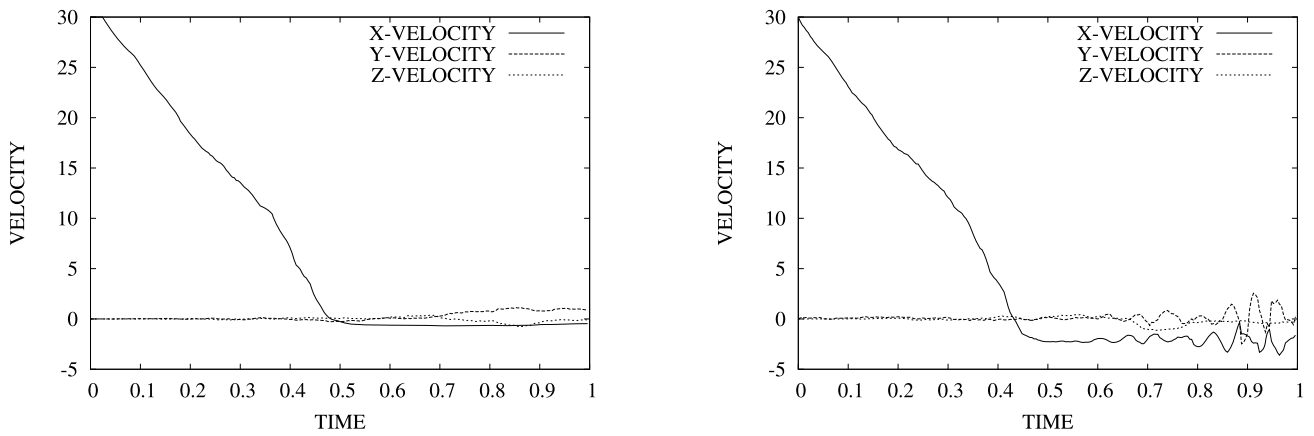


**Fig. 19** The CG-velocity. *Left*: charged. *Right*: charged with field (note the effects is helical-type spin). Note that only particles that are in the domain of interest are included in the computations

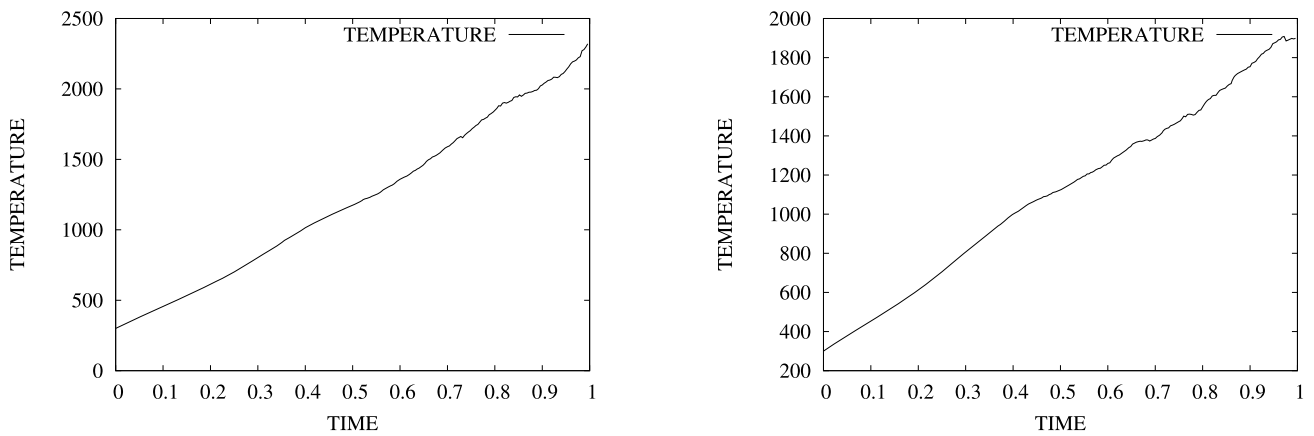


**Fig. 20** The temperature of the particles within the box. *Left*: charged and *Right*: charged with field. The temperature is higher in the case where no electromagnetic field is present, because of impact against the rigid foundation. Note that only particles that are in the domain of interest are included in the computations

As an example, consider the special case when  $\mathbf{v}(t = 0) = v_o \mathbf{e}_1$ ,  $\mathbf{B}^{ext} = B_3^{ext} \mathbf{e}_3$  and  $E^{ext} = E^{ext} \mathbf{e}_3$ , then

$$v_1(t) = v_o \cos \omega t \implies r_1(t) = \frac{v_o}{\omega} \sin \omega t, \tag{11.9}$$

where  $\omega = \frac{qB_3^{ext}}{m}$  is the cyclotron frequency,<sup>14</sup>  $\frac{v_o}{\omega} = \frac{v_o m}{qB_3^{ext}}$  is the radius of oscillation, and

$$v_2(t) = -v_o \sin \omega t \implies r_2(t) = \frac{v_o}{\omega} (\cos \omega t - 1), \tag{11.10}$$

and

$$v_3(t) = \frac{q}{m} E_3^{ext} t \implies r_3(t) = \frac{q}{2m} E_3^{ext} t^2. \tag{11.11}$$

This field generates helical motion. Notice that when  $E_3^{ext} = 0$ , this traces out the equation of a circle centered at  $(0, -\frac{v_o}{\omega} = -\frac{v_o m}{qB_3^{ext}})$ . The radius of the “magnetically-induced circle” is

$$\frac{v_o}{\omega} = \frac{v_o m}{qB_3^{ext}}. \tag{11.12}$$

Thus, if a desired “turning radius” is denoted by  $R$ , one may solve for the magnetic field that delivers the desired effect by computing  $B_3^{ext} = \frac{v_o m}{qR}$ . The smaller the radius, the larger the magnetic field must be. Also, the larger the initial momentum, the larger the magnetic field must be.

## 12 Closing Remarks

We close by commenting on an application not addressed earlier, namely *modern ignition systems in internal combustion engines*. Currently, the development of ignition systems for ultra-lean fuels, such as ethanol, is an area of high interest for spark (a localized electrical ion-jet) control. Because of the advancements in sensor and control systems in harsh environments (see Azevedo et al. [3] and Schwartz [123]), the real-time adjustment of in-situ ignition systems has emerged, and is an area of active research. In particular, spark dispersion and control via electromagnetic (microwave) techniques is now possible. Such approaches are important for developing hybrid systems involving compression ignition direct injection (CIDI) and homogeneous charge compression ignition (HCCI) engine platforms, in order to improve the performance of a broad class of engines. Such systems can lead to improved efficiency by igniting ultra-lean fuels at low temperatures where standard compression engines are limited and misfiring occurs. In

particular, it has recently been proposed that shortly after a spark (charged plasma) is discharged into the combustion chamber, a microwave is released to disperse the spark throughout the combustion chamber (Fig. 11). Because of the dispersion of the spark throughout the combustion chamber, the ignition system relies far less on the propagation of the flame to ignite the fuel and, hence, far leaner fuels may be employed without misfire occurring. As mentioned, until recently, the detailed control of sparks has been unreachable. However, within the last decade microtechnology, in particular microelectronic sensors, has made it possible for engineers control combustion events via the propagation of sparks and flame fronts. This is a large field, and we list a cross-section of that research for the interested reader: Ikeda et al. [50], Kaneko et al. [66], Liepold et al. [76], Phelps [109], Aleiferis et al. [2], Johansson [65], Kogoma [73], Phuoc [115], Morsy et al. [96], Morsy et al. [97], Ma et al. [89, 90], Mohamed et al. [95], Weinberg and Wilson [134], Dale et al. [18], Ronney [119], Beduneau [10], Chen and Lewis [17], Phuoc [116], Kim et al. [70, 71], Ombrello and Ju [102], Mintousov et al. [93], Korolev and Matveev [74], Esakov et al. [28], Linkenheil et al. [81, 82], Ikeda et al. [51], Kawahara et al. [68], Mehresh et al. [91], Bogin et al. [16] and Prager et al. [114]. A further understanding of what influences localized electrical jets is critical for the improvement of combustion processes. In many cases, the analysis of such sprays/jets require the simulation of the electromagnetic response, as well as its resulting coupled thermal response, which can be important to determine possible “hot spots” and to avoid non-uniform dispersion. The current work of the author involved in the development of models and numerical solution strategies to analyze the coupled response of such sprays/sparks in order to facilitate the creation of “designer sparks”.

An important aspect of any model is identification of parameters which force the system behavior to match a (desired) target response. For example, in the ideal case, one would like to determine the type of system parameters that produce certain overall responses, via numerical simulations, in order to guide or minimize time-consuming laboratory tests. A relatively straightforward way of achieving this is to consider inverse problems whereby particulate parameters are sought which deliver a desired overall behavior by minimizing a cost function. For example, a design problem can be set up by defining an  $n$ -tuple design vector, denoted  $\mathbf{\Lambda} \stackrel{\text{def}}{=} (\Lambda_1, \Lambda_2, \dots, \Lambda_n)$ , consisting of the following free system variables: (1) *Particulate masses*, (2) *Particulate volume fraction*, (3) *Particulate interaction laws*, (4) *Particulate velocities*, (5) *Particulate friction* and (6) *External electromagnetic fields* to minimize particulate agglomeration and maximize particulate dispersion. Generally, formulations of such objective functions will possess nonconvex and nondifferentiable dependency on the design variables

<sup>14</sup>The cyclotron frequency (gyrofrequency) is the angular frequency at which a charged particle makes circular orbits in a plane perpendicular to the static magnetic field.

(especially if there are constraints). The minimization of such objective functions can be achieved by using (non-derivative) “genetic” algorithms before applying classical gradient-based schemes. There are a variety of genetic algorithms, employing concepts of species evolution, such as reproduction, mutation and crossover. Such methods can be traced back, at least, to the work Holland [44]. For reviews of such methods, see Goldberg [34], Davis [19], Onwubiko [101], Kennedy and Eberhart [69] Lagaros et al. [75], Papadrakakis et al. [103–107] and Goldberg and Deb [35]. Such approaches have been extensively applied to related problems, involving randomly dispersed particulates in continuous media, in Zohdi [142–157].

## References

- Aboudi J (1992) Mechanics of composite materials—a unified micromechanical approach, vol 29. Elsevier, Amsterdam
- Aleiferis PG, Taylor AMKP, Whitelaw JH, Ishii K, Urata Y (2000) Cyclic variations of initial flame kernel growth in a Honda Vtec-E lean-burn spark-ignition engine. SAE Paper No 2000-01-1207
- Azevedo RG, Jones DG, Jog AV, Jamshidi B, Myers DR, Chen L, Fu X-A, Mehregany M, Wijesundara MJB, Pisano AP (2007) A SiC MEMS resonant strain sensor for harsh environment applications. *IEEE Sens J* 7(4):568–576
- Armero F, Simo JC (1992) A new unconditionally stable fractional step method for non-linear coupled thermomechanical problems. *Int J Numer Methods Eng* 35:737–766
- Armero F, Simo JC (1993) A-priori stability estimates and unconditionally stable product formula algorithms for non-linear coupled thermoplasticity. *Int J Plast* 9:149–182
- Armero F, Simo JC (1996) Formulation of a new class of fractional-step methods for the incompressible MHD equations that retains the long-term dissipativity of the continuum dynamical system, integration algorithms for classical mechanics. *Fields Inst Commun* 10:1–23
- Armero F (1999) Formulation and finite element implementation of a multiplicative model of coupled poro-plasticity at finite strains under fully saturated conditions. *Comput Methods Appl Mech Eng* 171:205–241
- Bathe KJ (1996) Finite element procedures. Prentice-Hall, New York
- Becker EB, Carey GF, Oden JT (1980) Finite elements: an introduction. Prentice-Hall, New York
- Beduneau JL, Kim B, Zimmer L, Ikeda Y (2003) Measurements of minimum ignition energy in premixed laminar methane/air flow by using laser induced spark. *Combust Flame* 132:653–665
- Behringer RP, Baxter GW (1993) Pattern formation, complexity & time-dependence in granular flows. In: Mehta A (ed) Granular matter—an interdisciplinary approach. Springer, New York, pp 85–119
- Behringer RP (1993) The dynamics of flowing sand. *Nonlinear Sci Today* 3:1
- Behringer RP, Miller BJ (1997) Stress fluctuations for sheared 3D granular materials. In: Behringer R, Jenkins J (eds) Proceedings, powders & grains 97. Balkema, Rotterdam, pp 333–336
- Behringer RP, Howell D, Veje C (1999) Fluctuations in granular flows. *Chaos* 9:559–572
- Berezin YA, Hutter K, Spodareva LA (1998) Stability properties of shallow granular flows. *Int J Nonlinear Mech* 33(4):647–658
- Bogin G, Chen JY, Dibble RW (2008) The effects of intake pressure, fuel concentration, and bias voltage on the detection of ions in a Homogeneous Charge Compression Ignition (HCCI) engine. In: Proc of the combustion institute, vol 32
- Chen YL, Lewis JW (2001) Visualisation of laser-induced breakdown and ignition. *Opt Express* 9(7):360–372
- Dale JD, Smy PR, Clements RM (1978) Laser ignited internal combustion engine—an experimental study. SAE-780329, Detroit
- Davis L (1991) Handbook of genetic algorithms. Thompson Computer Press, Washington
- Doltsinis ISt (1993) Coupled field problems—solution techniques for sequential & parallel processing. In: Papadrakakis M (ed) Solving large-scale problems in mechanics. Wiley, New York
- Doltsinis ISt (1997) Solution of coupled systems by distinct operators. *Eng Comput* 14:829–868
- Donev A, Cisse I, Sachs D, Variano EA, Stillinger F, Connelly R, Torquato S, Chaikin P (2004) Improving the density of jammed disordered packings using ellipsoids. *Science* 33:990–993
- Donev A, Stillinger FH, Chaikin PM, Torquato S (2004) Unusually dense crystal ellipsoid packings. *Phys Rev Lett* 92:255506
- Donev A, Torquato S, Stillinger F (2005) Neighbor list collision-driven molecular dynamics simulation for nonspherical hard particles-I. Algorithmic details. *J Comput Phys* 202:737
- Donev A, Torquato S, Stillinger F (2005) Neighbor list collision-driven molecular dynamics simulation for nonspherical hard particles-II. Application to ellipses and ellipsoids. *J Comput Phys* 202:765
- Donev A, Torquato S, Stillinger FH (2005) Pair correlation function characteristics of nearly jammed disordered and ordered hard-sphere packings. *Phys Rev E* 71:011105
- Duran J (1997) Sands, powders and grains. An introduction to the physics of granular matter. Springer, Berlin
- Esakov II, Grachev LP, Khodataev KV, Vinogradov VV, Van Wie DM (2006) Propane-air mixture combustion assisted by MW discharge in a speedy airflow. *IEEE Trans Plasma Sci* 34(6):2497
- Farhat C, Lesoinne M, Maman N (1995) Mixed explicit/implicit time integration of coupled aeroelastic problems: three-field formulation, geometric conservation and distributed solution. *Int J Numer Methods Fluids* 21:807–835
- Farhat C, Lesoinne M (2000) Two efficient staggered procedures for the serial and parallel solution of three-dimensional nonlinear transient aeroelastic problems. *Comput Methods Appl Mech Eng* 182:499–516
- Farhat C, van der Zee G, Geuzaine P (2006) Provably second-order time-accurate loosely-coupled solution algorithms for transient nonlinear computational aeroelasticity. *Comput Methods Appl Mech Eng* 195:1973–2001
- Fish J, Chen W (2003) Modeling and simulation of piezocomposites. *Comput Methods Appl Mech Eng* 192:3211–3232
- Frenklach M, Carmer CS (1999) Molecular dynamics using combined quantum & empirical forces: application to surface reactions. *Adv Class Traject Methods* 4:27–63
- Goldberg DE (1989) Genetic algorithms in search, optimization & machine learning. Addison-Wesley, Reading
- Goldberg DE, Deb K (2000) Special issue on genetic algorithms. *Comput Methods Appl Mech Eng* 186(2–4):121–124
- Goldsmith W (2001) Impact: the theory & physical behavior of colliding solids. Dover, New York
- Gray JMNT, Wieland M, Hutter K (1999) Gravity-driven free surface flow of granular avalanches over complex basal topography. *Proc R Soc Lond A* 455:1841–1874
- Gray JMNT, Hutter K (1997) Pattern formation in granular avalanches. *Contin Mech Thermodyn* 9:341–345
- Gray JMNT (2001) Granular flow in partially filled slowly rotating drums. *J Fluid Mech* 441:1–29

40. Greve R, Hutter K (1993) Motion of a granular avalanche in a convex & concave curved chute: experiments & theoretical predictions. *Philos Trans R Soc Lond A* 342:573–600
41. Haile JM (1992) *Molecular dynamics simulations: elementary methods*. Wiley, New York
42. Hase WL (1999) *Molecular dynamics of clusters, surfaces, liquids, & interfaces advances in classical trajectory methods*, vol 4. JAI Press, London
43. Hashin Z (1983) Analysis of composite materials: a survey. *ASME J Appl Mech* 50:481–505
44. Holland JH (1975) *Adaptation in natural & artificial systems*. University of Michigan Press, Ann Arbor
45. Hughes TJR (1989) *The finite element method*. Prentice Hall, New York
46. Hutter K (1996) Avalanche dynamics. In: Singh VP (ed) *Hydrology of disasters*. Kluwer Academic, Dordrecht, pp 317–394
47. Hutter K, Koch T, Plüss C, Savage SB (1995) The dynamics of avalanches of granular materials from initiation to runout. Part II. Experiments. *Acta Mech* 109:127–165
48. Hutter K, Rajagopal KR (1994) On flows of granular materials. *Contin Mech Thermodyn* 6:81–139
49. Hutter K, Siegel M, Savage SB, Nohguchi Y (1993) Two-dimensional spreading of a granular avalanche down an inclined plane. Part I: Theory. *Acta Mech* 100:37–68
50. Ikeda Y, Nishiyama A, Kaneko M (2009) Microwave enhanced ignition process for fuel mixture at elevated pressure of 1 MPa. In: 47th AIAA aerospace sciences meeting including the new horizons forum and aerospace exposition 5–8 January 2009, Orlando, Florida
51. Ikeda Y, Nishiyama A, Kawahara N, Tomita E, Nakayama T (2006) Local equivalence ratio measurement of CH<sub>4</sub>/air and C<sub>3</sub>H<sub>8</sub>/air laminar flames by laser-induced breakdown spectroscopy. In: 44th AIAA aerospace sciences meeting and exhibit, 9–12 January 2006, Reno, Nevada, AIAA Paper No 2006-965
52. Jackson JD (1998) *Classical electrodynamics*, 3rd edn. Wiley, New York
53. Jaeger HM, Nagel SR (1992) La physique de l'état granulaire. *Recherche* 249:1380
54. Jaeger HM, Nagel SR (1992) Physics of the granular state. *Science* 255:1523
55. Jaeger HM, Nagel SR (1993) La fisica del estado granular. *Mundo Cient* 132:108
56. Jaeger HM, Knight JB, Liu CH, Nagel SR (1994) What is shaking in the sand box? *Mat Res Soc Bull* 19:25
57. Jaeger HM, Nagel SR, Behringer RP (1996) The physics of granular materials. *Phys Today* 4:32
58. Jaeger HM, Nagel SR, Behringer RP (1996) Granular solids, liquids & gases. *Rev Mod Phys* 68:1259
59. Jaeger HM, Nagel SR (1997) Dynamics of granular material. *Am Sci* 85:540
60. Jenkins JT, Strack ODL (1993) Mean-field inelastic behavior of random arrays of identical spheres. *Mech Mater* 16:25–33
61. Jenkins JT, La Ragione L (1999) Particle spin in anisotropic granular materials. *Int J Solids Struct* 38:1063–1069
62. Jenkins JT, Koenders MA (2004) The incremental response of random aggregates of identical round particles. *Eur Phys J E Soft Matter* 13:113–123
63. Jenkins JT, Johnson D, La Ragione L, Makse H (2005) Fluctuations and the effective moduli of an isotropic, random aggregate of identical, frictionless spheres. *J Mech Phys Solids* 53:197–225
64. Johnson K (1985) *Contact mechanics*. Cambridge University Press, Cambridge
65. Johansson B (1996) Cycle to cycle variations in SI engines—the effects of fluid flow and gas composition in the vicinity of the spark plug on early combustion. SAE Paper 962084
66. Kaneko M, Nishiyama A, Jeong H, Kantano H, Ikeda I (2008) Combustion characteristics of microwave plasma combustion engine. In: Japanese society of automotive engineers, May, pp 7–11
67. Kansaal A, Torquato S, Stillinger F (2002) Diversity of order and densities in jammed hard-particle packings. *Phys Rev E* 66:041109
68. Kawahara K, Ueda K, Ando H (1998) Mixing control strategy for engine performance improvement in a gasoline direct-injection engine. SAE Paper No 980158
69. Kennedy J, Eberhart R (2001) *Swarm intelligence*. Morgan Kaufmann, San Mateo
70. Kim W, Do H, Cappelli M, Mungal M (2007) Plasma assisted methane premixed flame simulation using BOLSIG and OPPDIF. In: 45th AIAA aerospace sciences meeting and exhibit, 8–11 Jan 2007, Reno, Nevada, AIAA Paper No 2007-0379
71. Kim Y, Ferreri VW, Rosocha LA, Anderson GK, Abbate S, Kim K-T (2006) Effect of plasma chemistry on activated propane/air flames. *IEEE Trans Plasma Sci* 34(6):2532–2536
72. Koch T, Greve R, Hutter K (1994) Unconfined flow of granular avalanches along a partly curved surface. II. Experiments & numerical computations. *Proc R Soc Lond A* 445:415–435
73. Kogoma M (2003) Generation of atmospheric-pressure glow and its applications. *J Plasma Fusion Res* 79(10):1000
74. Korolev YD, Matveev IB (2006) Nonsteady-state processes in a plasma pilot for ignition and flame control. *IEEE Trans Plasma Sci* 34(6):2507
75. Lagaros N, Papadrakakis M, Kokossalakis G (2002) Structural optimization using evolutionary algorithms. *Comput Struct* 80:571–589
76. Leipold F, Stark RH, El-Habachi A, Schoenbach KH (2000) Electron density measurements in an atmospheric pressure air plasma by means of IR heterodyne interferometry. *J Phys D Appl Phys* 33:2268–2273
77. Lesoinne M, Farhat C (1998) Free staggered algorithm for nonlinear transient aeroelastic problems. *AIAA J* 36(9):1754–1756
78. Le Tallec P, Mouro J (2001) Fluid structure interaction with large structural displacements. *Comput Methods Appl Mech Eng* 190(24–25):3039–3067
79. Lewis RW, Schrefler BA (1998) *The finite element method in the static & dynamic deformation & consolidation of porous media*, 2nd edn. Wiley, New York
80. Lewis RW, Schrefler BA, Simoni L (1992) Coupling versus uncoupling in soil consolidation. *Int J Numer Anal Methods Geomech* 15:533–548
81. Linkenheil K, Ruoss RO, Heinrich W (2004) Design and evaluation of a novel spark-plug based on a microwave coaxial resonator. In: Microwave conference. 34th European, vol 3(11–15), pp 1561–1564
82. Linkenheil K, Ruoss HO, Grau T, Seidel J, Heinrich W (2005) A novel spark-plug for improved ignition in engines with gasoline direct injection (GDI). *Plasma Sci IEEE Trans* 33(5):1696
83. Liu CH, Jaeger HM, Nagel SR (1991) Finite size effects in a sandpile. *Phys Rev A* 43:7091
84. Liu CH, Nagel SR (1993) Sound in a granular material: disorder & nonlinearity. *Phys Rev B* 48:15646
85. Luo L, Dornfeld DA (2001) Material removal mechanism in chemical mechanical polishing: theory and modeling. *IEEE Trans Semicond Manuf* 14(2):112–133
86. Luo L, Dornfeld DA (2003) Effects of abrasive size distribution in chemical-mechanical planarization: modeling and verification. *IEEE Trans Semicond Manuf* 16:469–476
87. Luo L, Dornfeld DA (2003) Material removal regions in chemical mechanical planarization for sub-micron integration for sub-micron integrated circuit fabrication: coupling effects of slurry chemicals, abrasive size distribution, and wafer-pad contact area. *IEEE Trans Semicond Manuf* 16:45–56

88. Luo L, Dornfeld DA (2004) Integrated modeling of chemical mechanical planarization of sub-micron IC fabrication. Springer, Berlin
89. Ma JX, Alexander DR, Poulain DE (1998) Laser spark ignition and combustion characteristics of methane-air mixtures. *Combust Flame* 112:492–506
90. Ma JX, Ryan TW, Buckingham JP (1998) Nd:YAG laser ignition of natural gas. *ASME, 98-ICE-114*
91. Mehresh P, Souder J, Flowers D, Riedel U, Dibble RW (2005) Combustion timing in HCCI engines determined by ion-sensor: experimental and kinetic modeling. *Proc Combust Inst* 30:2701–2709
92. Michopoulos G, Farhat C, Fish J (2005) Survey on modeling and simulation of multiphysics systems. *J Comput Inf Sci Eng* 5(3):198–213
93. Mintousov E, Anokhin E, Starikovskii AY (2007) Plasma-assisted combustion and fuel reforming. In: 45th AIAA aerospace sciences meeting and exhibit, Jan 8–11, 2007, Reno, Nevada, AIAA Paper No 2007-1382
94. Moelwyn-Hughes EA (1961) *Physical chemistry*. Pergamon, Elmsford
95. Mohamed AH, Block R, Schoenbach KH (2002) Direct current discharges in atmospheric air. *IEEE Trans Plasma Sci* 30(1):182
96. Morsy MH, Ko YS, Chung SH, Cho P (2001) Laser-induced two point ignition of premixture with a single-shot laser. *Combust Flame* 125:724–727
97. Morsy MH, Chung SH (2003) Laser induced multi-point ignition with a single-shot laser using two conical cavities for hydrogen/air mixtures. *Exp Therm Fluid Sci* 27:491–497
98. Mura T (1993) *Micromechanics of defects in solids*, 2nd edn. Kluwer Academic, Dordrecht
99. Nagel SR (1992) Instabilities in a sandpile. *Rev Mod Phys* 64:321
100. Nemat-Nasser S, Hori M (1999) *Micromechanics: overall properties of heterogeneous solids*, 2nd edn. Elsevier, Amsterdam
101. Onwubiko C (2000) *Introduction to engineering design optimization*. Prentice Hall, New York
102. Ombrello T, Ju Y (2007) Ignition enhancement using magnetic gliding arc. In: 45th AIAA aerospace sciences meeting and exhibit, Jan 8–11, Reno, Nevada, AIAA Paper No 2007-1025
103. Papadrakakis M, Lagaros N, Thierauf G, Cai J (1998) Advanced solution methods in structural optimisation using evolution strategies. *Eng Comput J* 15(1):12–34
104. Papadrakakis M, Lagaros N, Tsompanakis Y (1998) Structural optimization using evolution strategies and neural networks. *Comput Methods Appl Mech Eng* 156(1):309–335
105. Papadrakakis M, Lagaros N, Tsompanakis Y (1999) Optimization of large-scale 3D trusses using evolution strategies and neural networks. *Int J Space Struct* 14(3):211–223
106. Papadrakakis M, Tsompanakis J, Lagaros N (1999) Structural shape optimisation using evolution strategies. *Eng Optim* 31:515–540
107. Papadrakakis M, Lagaros N, Tsompanakis Y, Plevris V (2001) Large scale structural optimization: Computational methods and optimization algorithms. *Arch Comput Methods Eng State Art Rev* 8(3):239–301
108. Park KC, Felippa CA (1983) Partitioned analysis of coupled systems. In: Belytschko T, Hughes TJR (eds) *Computational methods for transient analysis*. North-Holland, Amsterdam
109. Phelps AV (1987) Excitation and ionization coefficients. In: Christophourou LG, Bouldin DW (eds) *Gaseous dielectrics V*. Pergamon, Elmsford
110. Piperno S (1997) Explicit/implicit fluid/structure staggered procedures with a structural predictor & fluid subcycling for 2D inviscid aeroelastic simulations. *Int J Numer Methods Fluids* 25:1207–1226
111. Piperno S, Farhat C, Larroutourou B (1995) Partitioned procedures for the transient solution of coupled aeroelastic problems—part I: model problem, theory, and two-dimensional application. *Comput Methods Appl Mech Eng* 124(1–2):79–112
112. Piperno S, Farhat C (2001) Partitioned procedures for the transient solution of coupled aeroelastic problems—part II: energy transfer analysis and three-dimensional applications. *Comput Methods Appl Mech Eng* 190:3147–3170
113. Pöschel T, Schwager T (2004) *Computational granular dynamics*. Springer, Berlin
114. Prager J, Riedel U, Warnatz J (2007) Modeling ion chemistry and charged species diffusion in lean methane-oxygen flames. *Proc Combust Inst* 31(1):1129–1137
115. Phuoc T (2000) Single-point versus multi-point laser ignition: Experimental measurements of combustion times and pressures. *Combust Flame* 122:508–510
116. Phuoc T (2000) Laser spark ignition: experimental determination of laser-induced breakdown thresholds of combustion gases. *Opt Commun* 175:419–423
117. Rapaport DC (1995) *The art of molecular dynamics simulation*. Cambridge University Press, Cambridge
118. Rietema K (1991) *Dynamics of fine powders*. Springer, Berlin
119. Ronney PD (1994) Laser versus conventional ignition of flames. *Opt Eng* 33(2):510
120. Schlick T (2000) *Molecular modeling & simulation. An interdisciplinary guide*. Springer, New York
121. Schmidt L (1998) *The engineering of chemical reactions*. Oxford University Press, London
122. Schrefler BA (1985) A partitioned solution procedure for geothermal reservoir analysis. *Commun Appl Numer Methods* 1:53–56
123. Schwartz SW, Myers DR, Kramer RK, Choi S, Jordan A, Wijesundara MBJ, Hopcroft MA, Pisano AP (2008) Silicon and silicon carbide survivability in an in-cylinder combustion environment. In: *PowerMEMS 2008*, Sendai, Japan, Nov 9–12, 2008
124. Sukop MC, Thorne DT (2006) *Lattice-Boltzmann modeling: an introduction for geoscientists and engineers*. Springer, Berlin
125. Stillinger FH, Weber TA (1985) Computer simulation of local order in condensed phases of silicon. *Phys Rev B* 31:5262–5271
126. Szabo B, Babúska I (1991) *Finite element analysis*. Wiley Interscience, New York
127. Tabor D (1975) Interaction between surfaces: adhesion & friction. In: Blakely O (ed) *Surface physics of materials*, vol II. Academic Press, New York/San Francisco/London, Chap 10
128. Tai Y-C, Noelle S, Gray JMNT, Hutter K (2002) Shock capturing & front tracking methods for granular avalanches. *J Comput Phys* 175:269–301
129. Tai Y-C, Gray JMNT, Hutter K, Noelle S (2001) Flow of dense avalanches past obstructions. *Ann Glaciology* 32:281–284
130. Tai Y-C, Noelle S, Gray JMNT, Hutter K (2001) An accurate shock-capturing finite-difference method to solve the Savage-Hutter equations in avalanche dynamics. *Ann Glaciol* 32:263–267
131. Tersoff J (1988) Empirical interatomic potential for carbon, with applications to amorphous carbon. *Phys Rev Lett* 61:2879–2882
132. Torquato S (2002) *Random heterogeneous materials: microstructure and macroscopic properties*. Springer, New York
133. Tursa E, Schrefler BA (1994) On consistency, stability and convergence of staggered solution procedures. *Rend Mat Accad Lincei Rome* 9(5):265–271
134. Weinberg FJ, Wilson JR (1971) A preliminary investigation of the use of focused laser beams for minimum ignition energy studies. *Proc R Soc Lond A* 321:41–52
135. Widom B (1966) Random sequential addition of hard spheres to a volume. *J Chem Phys* 44:3888–3894

136. Wieland M, Gray JMNT, Hutter K (1999) Channelized free-surface flow of cohesionless granular avalanches in a chute with shallow lateral curvature. *J Fluid Mech* 392:73–100
137. Wriggers P (2002) *Computational contact mechanics*. Wiley, New York
138. Wriggers P (2008) *Nonlinear finite element analysis*. Springer, Berlin
139. Zienkiewicz OC (1984) Coupled problems & their numerical solution. In: Lewis RW, Bettes P, Hinton E (eds) *Numerical methods in coupled systems*. Wiley, New York, pp 35–58
140. Zienkiewicz OC, Paul DK, Chan AHC (1988) Unconditionally stable staggered solution procedure for soil-pore fluid interaction problems. *Int J Numer Methods Eng* 26:1039–1055
141. Zienkiewicz OC, Taylor RL (1991) *The finite element method*. Vols I and II. McGraw-Hill, New York
142. Zohdi TI (2002) An adaptive-recursive staggering strategy for simulating multifield coupled processes in microheterogeneous solids. *Int J Numer Methods Eng* 53:1511–1532
143. Zohdi TI (2003) Genetic design of solids possessing a random-particulate microstructure. *Philos Trans R Soc Math Phys Eng* 361(1806):1021–1043
144. Zohdi TI (2003) On the compaction of cohesive hyperelastic granules at finite strains. *Proc R Soc* 454(2034):1395–1401
145. Zohdi TI (2003) Computational design of swarms. *Int J Numer Methods Eng* 57:2205–2219
146. Zohdi TI (2003) Constrained inverse formulations in random material design. *Comput Methods Appl Mech Eng* 192(28–30):3179–3194
147. Zohdi TI (2004) Modeling and simulation of a class of coupled thermo-chemo-mechanical processes in multiphase solids. *Comput Methods Appl Mech Eng* 193(6–8):679–699
148. Zohdi TI (2004) Modeling and direct simulation of near-field granular flows. *Int J Solids Struct* 42(2):539–564
149. Zohdi TI (2004) A computational framework for agglomeration in thermo-chemically reacting granular flows. *Proc R Soc* 460(2052):3421–3445
150. Zohdi TI (2005) Charge-induced clustering in multifield particulate flow. *Int J Numer Methods Eng* 62(7):870–898
151. Zohdi TI (2006) Computation of the coupled thermo-optical scattering properties of random particulate systems. *Comput Methods Appl Mech Eng* 195:5813–5830
152. Zohdi TI (2007) Computation of strongly coupled multifield interaction in particle-fluid systems. *Comput Methods Appl Mech Eng* 196:3927–3950
153. Zohdi TI (2007) Particle collision and adhesion under the influence of near-fields. *J Mech Mater Struct* 2(6):1011–1018
154. Zohdi TI (2008) On the computation of the coupled thermo-electromagnetic response of continua with particulate microstructure. *Int J Numer Methods Eng* 76:1250–1279
155. Zohdi TI (2009) Mechanistic modeling of swarms. *Comput Methods Appl Mech Eng* 198(21–26):2039–2051
156. Zohdi TI (2007) *Introduction to the modeling and simulation of particulate flows*. SIAM, Philadelphia
157. Zohdi TI, Wriggers P (2008) *Introduction to computational micromechanics*, 2nd edn. Springer, Berlin